Early human fetal lung atlas reveals the temporal dynamics of epithelial cell plasticity

Henry Quach[1,2*], **Spencer Farrell**[3*], Kayshani Kanagarajah[1,2], Michael Wu[1], Xiaoqiao Xu[4], Prajkta Kallurkar[4], Andrei Turinsky[4], Christine E. Bear[5], Felix Ratjen[6], Sidhartha Goyal[3], Theo J. Moraes[6], Amy P. Wong[1,2]

[*] Co-first authorship, equal contributions

1. Program in Developmental and Stem Cell Biology, Hospital for Sick Children, 686 Bay Street, PGCRL 16-9420, Toronto, Ontario M5G0A4
2. Department of Laboratory Medicine & Pathobiology, University of Toronto
3. Department of Physics, University of Toronto
4. Centre for Computational Medicine, Hospital for Sick Children, Toronto, Canada
5. Program in Molecular Medicine, Hospital for Sick Children, Toronto, Canada
6. Program in Translational Medicine, Hospital for Sick Children, Toronto, Canada

Keywords: Lung development, Single-cell RNA and spatial transcriptomics, pluripotent stem cell differentiation, human fetal lung

Highlights:

1. Single-cell transcriptomics atlas from 19 human fetal lungs reveals cellular heterogeneity and previously unappreciated cellular plasticity in the epithelial compartment.
2. Identification of novel CFTR-expressing progenitor cells that gives rise to club, ciliated and PNEC.
3. Novel RNA velocity facilitated the identification of dynamic lineage trajectories in the epithelial compartment.
4. Temporally regulated cell autonomous and non-cell autonomous signaling may dictate cell lineage fates.
5. Integration of human pluripotent stem cell (hPSC)-derived fetal lung cells and organoids with primary lung dataset show hPSC-differentiations captures key developmental trajectories of fetal epithelial cell states.

Corresponding author:
Dr. Amy Wong, Program in Developmental and Stem Cell Biology, Hospital for Sick Children, 686 Bay Street, PGCRL 17-9704 Toronto, Ontario M5G0A4
Tel: 416-813-7654 x309334 | Email: apwong@sickkids.ca

Abstract

While animal models have provided key insights into conserved mechanisms of how the lung forms during development, human-specific developmental mechanisms are not always captured. To fully appreciate how developmental defects and disease states alter the function of the lungs, studies in human lung models are important. Here, we sequenced >150,000 single single-cells from 19 healthy human fetal lung tissues from gestational weeks 10-19 and identified at least 58 unique cell types/states contributing to the developing lung. We captured novel dynamic developmental trajectories from various progenitor cells that give rise to club, ciliated, and pulmonary neuroendocrine cells. We also identified four CFTR-expressing progenitor cell types and pinpointed the temporal emergence of these cell types. These developmental dynamics reveal broader epithelial cell plasticity and novel lineage hierarchies that were not previously reported. Combined with spatial transcriptomics, we identified both cell autonomous and non-cell autonomous signalling pathways that may dictate the temporal and spatial emergence of cell lineages. Finally, we showed that human pluripotent stem cell-derived fetal lung models capture cell lineage trajectories specifically through CFTR-expressing progenitor cells, that were also observed in the native fetal tissue. Overall, this study provides a comprehensive single-cell atlas of the developing human lung, outlining the temporal and spatial complexities of cell lineage development.

Introduction

Single-cell technologies are redefining the molecular signatures and functions of canonical cell types and identifying new cell types and cell states in organs and tissues[1,2]. Specifically, Single single-cell RNA sequencing (scRNA-seq) specifically has demonstrated revealed cellular transcriptomic heterogeneities and has enriched our understanding of how these cells contribute to development and disease. Over the past few years, there has been an explosion of single-cell atlases aimed at characterizing many post-natal and adult tissues and organs. Single-cell atlases of the adult human pulmonary system have illuminated the roles of key cell types in homeostasis and some diseases[3–6]. However, our understanding of the cells that form the developing fetal lung has largely been extrapolated from mouse studies[7,8], and not until recently have there been studies leveraging scRNA-seq to characterize the developing human fetal lung tissue[9,10]. While some conserved pathways regulating lung development are common between mouse and human, studies have identified species-specific differences in lung cell types and cellular distributions, which can impact function and disease pathogenesis. Understanding the molecular and cellular networks that drive the formation of the respiratory system during fetal development may provide important insight into regenerative processes during repair and potentially identify developmental origins of postnatal lung disease/disorders.

Recent sequencing datasets from a small collection of human fetal lungs obtained from early to mid-gestation normal fetuses, have highlighted some novel cell types and cell lineage trajectories[9,11] that are unique to human fetal development. Unfortunately, following up on these observations and their potential impact in post-natal lung function is hindered by experimentally tractable models.

Human pluripotent stem cells (hPSCs) are becoming a resourceful tool to generate "organoids" or in-vitro tissue mimetics to study fundamental mechanisms of human cell lineage development. Directed differentiation protocols towards mature lung epithelia[12–14] aim to recapitulate stepwise developmental milestones to ensure proper generation of specific cells and to date has achieved robust differentiations that are enabling cell therapy discoveries for the treatment of lung diseases such as Cystic fibrosis[15–17]. However, to precisely model the native tissue, a comprehensive understanding of the cells that exist and how they develop requires in-depth analysis of the native tissue. Understanding the developmental trajectories and pathways driving these cell lineage formations will also improve current hPSC differentiation protocols and generate bona fide cells for therapies.

Here, we present a comprehensive single-cell atlas of freshly isolated human fetal lungs from 19 independent lung samples spanning gestational weeks 10-19 and capturing >150,000 cells in total. Based on differentially expressed genes (DEG), we identified 58 cell types in the developing fetal lungs from the integrated datasets of all 19 lung samples. While the presence of canonical cell types previously found in both adult human lungs[4] and embryonic mouse lungs[8] were observed, we also identify novel cell types that are uniquely found in human fetal lungs including previously unidentified CFTR-expressing epithelial progenitor cells, a *PTEN+STAT3+* distal epithelial progenitor, and an uncommitted stromal cell-like epithelial cell that may be associated with stromal cell subtypes. Given the large number of cells sequenced from a

contiguous collection of fetal tissues, our dataset reveals important dynamic cellular plasticity and new lineage trajectories not previously identified. To determine cell lineage relationships and the ancestral origins of specific cell types, we leveraged our previously established modified RNA velocity prediction tool, LatentVelo[18], followed by partition-based graph abstraction (PAGA) visualization and *Slingshot*[19] to identify several novel trajectories and show the cellular transitions of the cells from different cell origins. We identified classical trajectories previously found in the immune, stromal and endothelial compartment, but we also uncovered novel unexpected trajectories especially in the developing epithelium. We revealed the dynamic nature of how CFTR-expressing epithelial progenitors contribute to the pulmonary neuroendocrine and multi-ciliated lineages. Moreover, in combination with spatial transcriptomics, we revealed cell autonomous and non-cell autonomous cell signalling pathways that specifically contributed to differing cell fates derived from a novel *SCGB3A2+SFTPB+CFTR+* cell population. Finally, we show that hPSC-derived fetal lung epithelia models capture several unique epithelial cell progenitors and lineage trajectories observed in the native fetal airways and supports the validity of hPSC-derived fetal lung models for future studies in specific cell lineage development and function in the developing lung.

Results

Identification of at least 58 distinct cell types in the developing human fetal lungs.

A total of 19 freshly isolated fetal lung tissues from elective pregnancy terminations from gestational weeks (GW)10-19 were collected and processed for 3' single-cell RNA sequencing (scRNA-seq) using from 10X Genomics. One sample was sampled twice from different regions of the lung to capture more cells representing from the upper and lower lungs (denotated with an asterisk, **Supplementary Table 1**). A total of 170,256 single-cells were sequenced at approximately 60,000 read depth per cell. FASTQ files were generated, and the reads were aligned with human reference genome hg38 (GRCh38) (**Extended Data Fig. 1A)**. After the removal of low-quality cells, dead cells, and doublets, 156,698 cells were analyzed. After normalization and dimensionality reduction, reciprocal principal component analysis (rPCA) was used to identify anchors for integration to generate the fetal lung dataset. Based on the expression of the male sex-determining genes*, SRY and DDX3Y*, and the X-chromosome inactivation gene, *XIST*, 12 male and 7 female lungs were collected (**Fig. 1A**). Leiden clustering informed by *Clustree*[20] was used to unbiasedly define the number of cell clusters (**Extended Data Fig. 1B**). Differentially expressed genes (DEG) based on non-parametric Wilcoxon rank sum test were used to annotate the cell populations which were broadly classified into 5 uniquely different cell populations (**Fig. 1B** and **Supplementary Table 2**) designated as stromal (N = 98,166; *COL1A1, COL1A2*), epithelial (N = 16,068; *EPCAM*), endothelial (N = 13,376; *PECAM1*), immune (N = 16,258; *CD74, CD3, NKG7*), and Schwann cells (N = 512; *NRXN1, S100B, PLP1*) (**Fig. 1C**). Further sub-clustering of each main cell population was informed by *Clustree* and DEG which resulted in a total of 58 distinct cell types/states identified in the developing lungs (**Fig. 1D**). Assessing the cell proportions over gestational time showed stromal cells formed the largest proportion of cells throughout the 10 weeks of development (**Extended Data Fig. 1C**). Myeloid and lymphoid cells emerged around

GW13 and gradually increased thereafter. Temporal assessment based on the gestational week of the lung tissues highlights the dynamic changes of cell populations (immune cells, red hatched box), with emergence of cells (ciliated cells, black hatched box), and temporal disappearance (specific epithelial subpopulations, green hatched box) of cell types over time (**Fig. 1E**). Considering the differences in number of cells captured for each gestational week, cell type proportions of these cell types similarly showed changes in the presence of varying cell types **(Supplementary Table 3).**

We next performed an integrated analyses to identify similarities and differences between our dataset and two recently published datasets encompassing similar developmental lung tissues[9,10]. Integrated UMAP overlay of our dataset (in red, **Fig. 1F**) with the published two datasets by He et al.[9], and Sountoulidis et al.[10], (combined, in grey) showed that 51 of the 58 cell clusters (~88%) were common amongst all three datasets (**Fig. 1G** and **Extended Data Fig. 1D**). However, 7 unique cell types were exclusively captured in our dataset and these included aerocytes and erythrocyte-like cell 1 from the endothelial cluster, monocyte 2 from the immune cluster, and stromal-like 1, stromal-like 2, ciliated cell precursor, and SMG basal cell in the epithelial cluster. This may reflect the larger cell number or the comprehensive range of fetal tissue that enabled us to capture these cell types/states. While He et al.[9] identified "aerocytes" and SMG basal cells in their dataset, differences between He et al.'s and our dataset's cell type classification are present. Interestingly, our dataset captured developing aerocytes (*TBX2, EDNRB, APLN*) that appeared as early as GW10, whereas He et al. only captured more mature aerocytes (TBX2, S100A3) at GW22. Differences in SMG basal cells can be accounted by unique inclusion of *CNN1, LGALS3,* and *LGALS1* in our dataset[21].

We next compared our fetal lung dataset to published single-cell atlas from human adult lung[4] using *MapQuery* function in Seurat to map query cells onto our reference fetal lung dataset. While we only identified 47% cell types that were shared between our dataset and the adult lung dataset (**Extended Data Fig. 1E**), it is plausible that there are more significant common cell types shared that have not been captured due to the limited sample size of the reference adult lung dataset. On the contrary, we also capture unique fetal lung cell (ie. Budtip progenitors, and several CFTR+ progenitor cells that will be discussed later in the description of the subpopulations). Cells that are common between fetal and adult lung tissues include many of the canonical cell types including endothelial subtypes, immune cells, and some epithelial subtypes (SMG secretory and basal cells, airway basal cells, and ciliated cells).

We also compared our dataset to a previous mouse embryonic lung single-cell atlas[8] and found 45% common cell types (**Extended Data Fig. 1F**). Notable similarities in the cells captured from the mouse dataset included several endothelial, immune and stromal subtypes. It should be noted that the mouse lung dataset by Negretti et al captures a broad range of tissues from embryonic day 12 (equivalent to the pseudoglandular lung tissues in mice). The large number of cells not captured in our fetal lung dataset that are found in the mouse embryonic lung dataset may be attributed to the differences in developmental stages of the tissue, which would capture different cell types/states. Other explanations include discordance in cell cluster annotation and differences

in single-cell preparation, including MACS enrichment that excluded specific cell types.

Conserved developmental trajectories of lipofibroblasts and airway fibroblasts in the developing lung stroma.

Stromal cells formed the largest proportion of cells in all lung tissues analyzed (**Fig. 1B**). We identified 10 stromal cell subtypes (**Fig. 2A**) based on DEG expression (**Supplementary Table 2**). These included lipofibroblasts, lipofibroblast precursors, cycling fibroblasts, early fibroblasts, airway fibroblast progenitors, uncommitted cells, airway smooth muscle cells (SMC), vascular SMC, chondrocytes, and an unknown stromal cell population. Lipofibroblasts and their precursors were the most abundant stromal cell type across all gestational weeks (**Fig. 2B**). Both cell types expressed abundant *TCF21*, previously shown in both mouse fetal and adult lung lipofibroblasts[22]. Lipofibroblast precursors differentially expressed higher levels of several canonical mesenchymal associated genes including the pleckstrin homology domain family H member 2 (*PLEKHH2),* and the microtubule actin cross-linking factor (*MACF1*) (**Fig. 2C**) as previously shown in mouse lipofibroblasts cell lineages[23]. Lipofibroblasts expressed progressively higher levels of the transcription factors *JUN, FOS* and *EGR1* (**Fig. 2D**), which are known to regulate the synthesis of structural extracellular matrices (ECM) such as collagen and elastin which are important in alveolar development[24]. While alveolar development occurs later in gestation, it is conceivable that lipofibroblasts in early fetal lung development play a role in laying down the ECM proteins required to form the airway structures. Differential enrichment analysis of the transcription factors driving these cell lineages showed an enrichment of *JUN*, *FOS,* and *IRF1* expression in lipofibroblasts and *STAT2* and *GATAD1* expression in lipofibroblast precursors.

Cycling fibroblasts and early fibroblasts were also present at a relatively high proportion in the early lung tissues (GW 10-14; ~6-10% and ~9-12% respectively) but gradually reduced in later gestational lung tissues (GW15 onwards; ~2-5% and ~3-7% respectively) (**Fig. 2B, Supplementary Table 3**). Other than the common collagen genes (*COL1A1, COL1A2*), cycling fibroblasts expressed high levels of genes associated with cellular proliferation *TOP2A, CENPF, MKI67* (**Fig. 2C**). Early fibroblasts expressed high levels of genes associated with chromatin remodeling such as *HELLS* and *TYMS*[25](**Fig. 2D**), previously shown to be highly expressed in mouse embryonic fibroblasts. The transcription factors differentially expressed in these cells include *E2F7, FOXM1* (known regulators of cell cycle in fibroblasts[26]) and *MYBL2*, a regulator of cell cycle progression, respectively. Interestingly, tight regulation of *MYBL2* has previously been shown to be critical in somatic reprogramming of mesenchymal to epithelial transitions[27], suggesting a potential contribution of these stromal cells to the epithelium.

There was also a significant proportion of uncommitted cells that were closely associated with cycling fibroblasts and lipofibroblast precursors based on the UMAP projections (**Fig. 2A**). These uncommitted cells share some transcriptional similarities to cycling fibroblasts and lipofibroblast precursors (**Fig. 2C**), but uniquely expressed high levels of the tissue inhibitor of matrix metalloproteinases *(TIMP3)* and galectin-3 *(LGALS3),* both involved in regulating the inflammatory responses[28,29]. Further investigation into differentially expressed transcription factors in these cells showed uniquely higher expression of *SOX2* and *NRD1*, the latter previously associated with tumor-induced fibroblast activation[30]. Airway fibroblast progenitors expressed higher levels of *SERPINF1, FBN1, IGFBP5.* Based on the elevated expression of these genes, airway fibroblasts appear to emerge around GW15 and uniquely expressed the transcription factor

HOXA10 (**Fig. 2D**). Airway SMC differentially expressed higher levels of *TAGLN, ACTA2, MYH11*, while vascular SMC expressed *IGFBP7, MEF2C, EGFL6*, both similarly reported in other studies[9]. Transcription factors differentially expressed in airway and vascular SMC included the zinc finger E-box binding homeobox 1 (*ZEB1),* a core EMT transcription factor[11], and the ETS variant transcription factor (*ETV1)*, which regulates cell growth, proliferation and differentiation, respectively. Chondrocytes differentially expressed many of the collagen genes including *COL2A1, COL11A1, COL9A*1 and the transcription factor CAMP Responsive Element Binding Protein 3 Like 2 (*CREB3L2* known regulate chondrocyte development. An unknown small cluster of stromal cells with distinct DEG expressed high levels of *AHSP, ALAS,* and *BPGN*, genes correlated with erythroid cells. They also expressed abundant levels of TMEM158, a gene enriched in cells undergoing epithelial-to-mesenchymal transition through STAT3 signalling[31]. The role of these unknown cells in fetal lung remains to be determined.

We further performed spatial transcriptomics using 10X' Visium technology and confirm the localization of airway fibroblast progenitors, lipofibroblast precursors, and airway SMC in GW15 and 18 fetal lung tissues (**Extended Data Fig. 2**). Early fibroblasts, lipofibroblasts, lipofibroblast precursors, and airway SMC are broadly distributed throughout the GW15 and GW18 fetal lungs. In contrast, airway fibroblast progenitors are primarily concentrated around the large airways, a region where lipofibroblast precursors are distinctly absent. This spatial distribution suggests that early fibroblasts, lipofibroblasts, lipofibroblast precursors, and airway SMC contribute broadly to lung development, whereas airway fibroblast progenitors contribute specifically to airway development.

To infer developmental lineages of the fibroblast clusters, we used LatentVelo to estimate RNA velocities and visualized these velocities on the UMAP embedding and with PAGA (**Fig. 2E, F**). Inferred trajectories suggested that cycling fibroblasts form early fibroblasts and uncommitted cells that then form into airway fibroblast progenitors and lipofibroblasts. We further validated these trajectories with Slingshot, using cycling fibroblasts as the "root cells", or cell origins and found a gradual change in gene expression as the cells along a differentiation trajectory to lipofibroblasts and airway fibroblast progenitors (**Fig. 2G, H**). To determine whether these trajectories changed over time, we grouped the datasets based on gestational time (Early: GW10-13, Mid: GW14-16 and Late: GW17-19) but found no changes in these trajectories when subsetting the analyses by GW (data not shown).

Identification of novel CFTR-expressing progenitor cells and temporal changes in epithelial cell fate dynamics.

Analysis of the top DEG and highly expressed canonical epithelial genes associated with specific epithelial cell types revealed 19 subtypes (**Fig. 3A, B** and **Supplementary Table 2**). Many of the epithelial cell types were found in all lung tissues except for ciliated cell precursors which emerged around GW13 onwards. Mature ciliated cells and *SCGB3A2+FOXJ1+* cells emerged around GW14 whereas basal cells and SMG secretory cells emerged around GW15, but these latter cell types represented only a very small fraction (~0.2-1% and ~1-5%) of the total epithelial cell population (**Supplementary Table 3, Extended Data Fig. 3A**). Pulmonary neuroendocrine cells

(PNEC) and *SOX2^{high}CFTR+* cells were found in higher abundance in early fetal lungs (<GW13) and then decreased in proportion in later gestational tissues.

Leveraging the expression of *SOX2* and *SOX9* to determine proximal and distal airway cells respectively[32], we identified subclusters that expressed relatively higher levels of *SOX2* and include PNEC, mature ciliated cells and their precursors, club cells, SC*GB3A2+FOXJ1+,* a CFTR-expressing cell type that co-expressed *SCGB3A2* and *SFTPB* (*SCGB3A2+SFTPB+CFTR+*[33]), and *SOX2^{high}CFTR+* cell populations (**Extended Data Fig. 3B**). On the contrary, *SOX9^{high}* cells included early alveolar type 2 (AT2)-like cells, budtip progenitors, *NKX2-1+SOX9+CFTR+* cells and both the stromal-like cell populations. Cells that expressed relatively lower levels of both *SOX2* and *SOX9* included submucosal gland (SMG) basal cells, SMG secretory cells, and a calmodulin-binding protein neurogranin *(NRGN)*-expressing cells. Interestingly, while *SOX2* and *SOX9* co-expressing cells have previously been identified in double positive distal tip lung progenitors[34], the expression of *SOX2* in the budtip progenitors in our dataset is relatively low compared to *SOX9*. Instead, cells that appeared to express both *SOX2* and *SOX9* at relatively equal levels included *SOX2^{low}CFTR+* cells, *PTEN+STAT3+* cells, basal cells, and the proliferating progenitors.

Proliferating progenitors were identified by the elevated expression of genes associated with cellular proliferation *MKI67,* and cell cycle genes encoding the microtubule-binding protein *CENPF, NUSAP1,* and *CDK1* (**Fig. 3B**)**.** Proliferating progenitors expressed abundant levels of *BRCA1* and *FOXM1,* and high levels of *TEAD4*, a downstream effector of the Hippo pathway involved in lung development[35]. Other than abundant expression of genes associated with cell proliferation (*TOP2A* and *CENPF*), these cells are relatively uncommitted.

An unknown epithelial cell cluster was found that expressed high levels of mTOR-related *STAT3* and *PTEN* (*PTEN+STAT3+*); no other cell-type-specific genes were differentially expressed in these cells. In the developing mouse lungs, mTOR signaling is required for *SOX2* acquisition and conversion of *SOX9+* distal progenitors to *SOX2+* proximal cells[36]. It is unclear if these *PTEN+STAT3+* cells are equivalent to transitional cells of distal to proximal progenitors, however these cells express DEG associated with cell cycle progression such as nuclear factor kappa B (*NFKB1)*, NFKB subunit (*REL)* and IFN regulatory factor 1 *(IRF1)* (**Extended Data Fig. 3C**). Selecting Visium dots with high proportion of *PTEN+STAT3+* cells show co-occurrence (or close proximity) with *NKX2-1+SOX9+CFTR+* cells and AT2-like cells in GW15 tissues, and only with *NKX2-1+SOX9+CFTR+* in GW18 tissues, suggesting these cells may reside near the developing airway bud (**Fig. 3E**). *PTEN+STAT3+* cells also express abundant levels of thrombospondin 1 (*THBS1,* **Supplementary Table 2**), an extracellular glycoprotein involved in cell-matrix and cell-cell interactions. Immunostaining for THBS positivity showed abundant and uniform expression in the developing bud especially in the early (GW12) lung (**Extended Data Fig. 3D**). In later tissues (GW15 and GW18) expression of THBS1 were found on the apical membrane of some epithelial cells in the developing airways and along the basement membrane of the larger airways.

A novel finding was the identification of four epithelial cell types that expressed relatively high levels of *CFTR* (**Extended Data Fig. 3B**). These include *NKX2-1+SOX9+CFTR+*, SOX2^{high}*CFTR+*, SOX2^{low}*CFTR+* and *SCGB3A2+SFTPB+CFTR+* cell populations. The *SOX2^{low}CFTR+* share many common DEG with *SOX2^{high}CFTR+* cells, however relative to

SOX2^{high}CFTR+ cells, *SOX2^{low}CFTR+* cells differentially expressed *GPRC5A* (a G protein-coupled receptor class C group 5 member A), involved in retinoic acid signaling, a pathway instrumental in lung development[37] (**Fig. 3B** and **Supplementary Table 2**). Spatial transcriptomics show an abundance of the Early AT2-like and *SOX2^{high}CFTR+* in the developing airways at GW15 (pie chart inset shows the proportion of cell types in the spatial region demarcated in the red dot of the H&E stain which contains the predominant respective cell type (asterisk, **Fig. 3D**). On the contrary, *SOX2^{low}CFTR+* cells are rare and found in the developing stalks of the airways. In later tissues (GW18), *NKX2-1+SOX9+CFTR+* cells appear to dominate all the developing airways, likely due to the large expansion in the number of airways formed at this point (**Extended Data Fig. 4A**). It is important to note that within a spatial area (demarcated in the Visium as dots) there is a heterogenous proportion of cell types that reside in that "focal" area. Using immunofluorescence staining, we determined that the TTF1+ or (NKX2-1) SOX9+CFTR+ cells were found mainly in the developing lung bud region (green hatched area), and with SOX9^{low} cells were found in the developing stalk region (red boxed region) (**Fig. 3E**). On the contrary, TTF1+SOX2+CFTR+ cells were found in the fetal airways with distinct clusters of SOX2^{high} (orange arrow) and SOX2^{low} (white hatched area) cells. The role of CFTR in the developing lung is unclear. However, previous studies in porcine fetal lungs suggest a role of CFTR in branching morphogenesis[38]. Transcription factors (**Extended Data Fig. 3C**) highly enriched in *SOX2^{high}CFTR+* cells included *RBPJ,* the transcriptional effector of NOTCH signalling[39], and *FOXA2,* which mediates branching morphogenesis and differentiation[40]. Interestingly, these cells also express high levels of *CD47* (**Supplementary Table 2**), a cell surface molecule used to enrich for multipotent human induced pluripotent stem cells (hiPSC)-derived lung progenitors[41]. *NKX2-1+SOX9+CFTR+* cells expressed high levels of *CPM*, *SFTPA*, *FGFR2,* and *MUC1* and the transcription factor *SMAD6*. SMAD signalling is important in alveolar stem cell development[42], which suggests *NKX2-1+SOX9+CFTR+* may be an ancestral source of alveolar cells, as has previously been suggested[43]. Indeed, *CPM* has previously been identified as a cell surface molecule used to enrich for fetal lung epithelial progenitors generated from hiPSC that can generate alveolospheres[44].

The *SCGB3A2+SFTPB+CFTR+* cells were found scattered throughout the airways (white dashed region, **Fig. 3F**). The transcription factors enriched in *SCGB3A2+SFTPB+CFTR+* cells included *CREB3L2* and *RUNX2* (**Extended Data Fig. 3C**), the former previously shown to regulate secretory cells[45] and the latter previously shown to be a regulator of goblet cell differentiation[46]. This would suggest the *SCGB3A2+SFTPB+CFTR+* cells share a lineage relationship with secretory cells[47].

Unlike in the adult lungs[3,48], fetal secretory, ciliated, and SMG cells expressed relatively low levels of *CFTR.* The rare ionocytes which express the highest levels of *CFTR* in postnatal lung tissues[48] was not detected in any of the fetal epithelia examined here. While this does not suggest that these cells do not exist during fetal lung development, the canonical genes (coexpression of *FOXI1* and *CFTR*) used to identify ionocytes could not isolate a distinct ionocyte-like population. Fetal club cells expressed high levels of the canonical genes *SCGB1A1, SCGB3A2,* and *CYB5A* (**Supplementary Table 2**) typically found in mature club cells. On the contrary, *SCGB3A2+FOXJ1+* cells expressed abundant genes associated with ciliogenesis (*RSPH1, DNAH5*) cells and would suggest these may be transitory cells originating from a secretory precursor.

Ciliated cell precursors and mature ciliated cells shared expression of several key genes including *DNAH5,* a protein-coding gene for microtubule assembly, *FOXJ1*, a key regulator of cilia gene expression, and *RSPH1*, a gene encoding a protein that localizes cilia **(**Cluster 10, **Fig. 3B).** Both cell types also expressed high levels of the transcription factor *TP73* (**Extended Data Fig. 3C**), an activator of ciliary marker *FOXJ1*[49]. Ciliated cell precursors however expressed high levels of *FOXN4* (**Supplementary Table 2**)*,* a transcription factor required for expression of motile cilia genes and observed in cells undergoing ciliated cell differentiation[50]. Mature ciliated cells, on the other hand, expressed prominent levels of the *TUBA1A* required for ciliogenesis[51]. Interestingly, we found a unique cell cluster that co-expressed *SCGB3A2* and *FOXJ1* (*SCGB3A2+FOXJ1+*) which were found dispersed in the airways (**Extended Data Fig. 3E**). The relationship between these cells with ciliated cells remains to be experimentally determined however assessment of the proximity scores of the cells from spatial transcriptomics suggest *SCGB3A2+FOXJ1+* cells are closely with associated with proximal cells including *SCGB3A2+SFTPB+CFTR+* and SOX2+ cells (**Fig. 3C**), suggests a lineage relationship between these cells. Below, we infer this relationship with RNA velocity.

Airway submucosal gland (SMG) basal cells expressed high levels of *IGFBP, TIMP3, LGALS1, LGALS3, S100A4,* and *S100A6,* all previously associated with SMG basal cells[9]. Similarly, SMG secretory cells expressed high levels of *UPK3B, RARRES2, C3,* and *ALDH1A2*. Both SMG basal and SMG secretory cells shared enriched expression of the *HOX* family transcription factors *HOXB5, HOXB2, HOXB4* and *HOXA5* (**Extended Data Fig. 3C**), all previously shown to regulate proximal-distal patterning and epithelial differentiation in the developing mouse airways[52].

Early AT2-like cells and budtip progenitors both expressed genes related to surfactant protein production such as *SFTPC, SFTPA1,* and *ABCA3.* Budtip progenitors also expressed high levels of *CA2, TESC, ETV5* as previously identified[53], in addition to *CCN1, CCN2*, *ITGA2*, genes associated with cellular proliferation *(EGR1*, *FOSB*), anti-apoptotic gene (*MCL1),* and *NFKBIA*. Budtip progenitors were found to be enriched with transcription factors *NFKB1* and *SOX9* (**Extended Data Fig. 3C**)*,* both involved in distal epithelia differentiation[54]. Early AT2-like cells on the other hand, expressed high levels of *MFSD2A*, *CPM*, and *IGFBP7*. Transcription factors enriched in early AT2-like cells included *ETV1* and *HNF1B*, as previously described[55] as well as *SOX9* and *FOXP2.* While ETV5 was previously shown to regulate human distal lung identity[11] and mouse adult lung AT2 identity[56], here we identify the homologous ETV1 as abundantly expressed in human fetal AT2-like cells. Proximity score analysis showed budtip progenitors and AT2-like cells were closely associated, suggesting these cells may also share regionally the same space (**Fig. 3C** and **3E**).

Other epithelial cell populations that are less defined and make up a smaller proportion of the total epithelium include the *NGRN+* cells that expressed abundant levels of *CCL5, TGFB1, GNG11,* which would suggest these cells may play a role in immunity and inflammation. However, their precise role in development has yet to be determined. Two stromal-like epithelial cell populations were also found in all fetal lung tissues examined. These cells were annotated based on the DEG of stromal associated genes including *COL3A1* which is expressed in squamous cell types[57]. Stromal-like cells 2 also expressed the mesenchyme homeobox 2 (*MEOX2*)[58] which regulates TGFbeta signalling pathway and epithelial-mesenchymal cell transition. These cells also express abundant *WNT2*, previously shown to orchestrate early lung morphogenesis[59]. Like the

NGRN+ cells, future studies will need to define the functional role of the stromal-like cells in the developing lung.

Similar to previous studies[9,10], PNEC emerged early in the developing lungs but the proportion of PNEC appeared to decrease to relatively low proportions by the end of the pseudoglandular stage (**Extended Data Fig. 3A**). PNEC expressed high levels of the canonical genes including *CHGB, CALCA,* and *ASCL1* (**Fig. 3B**) and the transcription factors *NEUROD1* and *ASCL1* were most abundantly expressed in these cells (**Extended Data Fig. 3C**), confirming their cell identity as previously described[9,10,60]. These cells were found in the airways (**Extended Data Fig. 4B**). Importantly, two PNEC subpopulations separated by differential expression of *ASCL1* and *CALCA* respectively was also observed in our dataset (**Extended Data Fig. 4C**) and previously identified[9].

In comparing the epithelial compartment to other recently published datasets of similar gestational ages, the ciliated cell precursors were not captured in the dataset by Peng et al.[9], and Sountoudilis et al.[10], (**Extended Data Fig. 4D** and **4E**, respectively). Moreover, SMG secretory and both SMG and airway basal cell populations were not found in the Sountoudilis et al. dataset. This may reflect differences in clustering resolutions or cluster annotations.

Using LatentVelo, we predicted the lineage relationships of the epithelial cell types (**Fig. 4A**). We also use a separate pseudotime method to arrive at these same results for validation (**Extended Data Fig. 5A**). Analyzing LatentVelo velocities with *CellRank*[61] reveals 3 terminal states: Mature ciliated cells, PNEC, and budtip cells **(Fig. 4B,** and **Extended Data Fig. 5B** and **C**). These identified terminal budtip cells are all at later GWs (GW 16-18). Using slingshot, we identified a bifurcation in the development at early budtip cells towards either the late budtip cells, or Early AT2-like cells and *NKX2-1+SOX9+CFTR+* cells (**Extended Data Fig. 5D**).

Based on PAGA using LatentVelo velocities, we observed trajectories that suggested a high degree of cellular plasticity of the proximal epithelial compartment as several trajectories would converge on the same cell types, in particular the identified terminal PNEC and mature ciliated states (**Fig. 4C**). We hypothesized that epithelial lineage development may be temporally regulated, and therefore to unmask these dynamic events, we needed to dissect the analysis based on developmental vignettes. Based on the emergence of several canonical cell types, such as mature ciliated cells and the significant decline of PNEC cells at ~GW14 (**Extended Data Fig. 3A**), we decided to group the tissues into 3 vignettes: Early (GW10-13), Mid (GW14-16), and Late (GW17-19). The late vignette (GW17-19) marks the early canalicular stage of lung development, a period in which differentiation and emergence of specific cell types emerge. A few noteworthy trajectories were observed. First, in early gestational tissues, there were multiple sources of PNEC contributions including 1) a trajectory that goes through stromal-like 1 cells to PNEC; and 2) a trajectory from budtip progenitors through to *SOX2^{high}CFTR* to *SCGB3A2+SFTPB+CFTR+* and then PNEC[33]. Changes in the DEG showed the gradual cell fate changes as the cells eventually gained expression of genes related to PNEC differentiation including *ASCL1* and *GHRL* (**Fig. 4E**). However, all of the PNEC trajectories weakened in the late stages. Several trajectories seemed to converge onto *SCGB3A2+SFTPB+CFTR+* in "mid" gestational tissues (**Fig. 4D**). These include cell sources from *SOX2^{low}CFTR+* cells, *SOX2^{high}CFTR+,* stromal-like cell 2, proliferating progenitors and basal cells. A strong connection (thick arrow line) between *NKX2-1+SOX9+CFTR+* and *SOX2^{high}CFTR+* cells and the latter with *SCGB3A2+SFTPB+CFTR+* were

observed in all timepoints, suggesting these cells are developmentally related. While a connection was observed between *NKX2-1+SOX9+CFTR+* and *SOX2^{low}CFTR+* cells, this weakened in late tissues. Similarly, a connection between budtip progenitors and *SOX2^{low}CFTR+* cells were also observed in all timepoints. Interestingly, the connection between budtip to AT2-like cells appeared to reflect only a subpopulation of budtip cells that emerged later in development (mid stage). During the mid (GW14-16) timepoints, the emergence and trajectories for mature ciliated cells are observed, stemming from budtip progenitors through stromal-like 1, club, and ciliated precursor cells or through *SCGB3A2+SFTPB+CFTR+* cells and *SCGB3A2+FOXJ1+* cells (**Fig. 4F**). Fetal club cells appeared to contribute to the ciliated cell precursor (**Fig. 4D**) supporting the notion that Club cells may have greater developmental potential as has been observed in mouse lung injury models[62]. Interestingly, there were no connections between fetal basal cells and club cells before GW17, which may be explained by the low numbers of basal cell captured for our analysis. In late tissues, trajectories originating from basal cells contribute to PNEC and Club cell lineages (**Fig. 4G**), suggesting the basal cells at this stage have acquired developmental plasticity similar to that observed in adult basal cells[63]. However, similar to He et al., we are unable to predict the origin of these basal cells[9], likely due to the low numbers of basal cells.

The plasticity of SCGB3A2+SFTPB+CFTR+ cells in PNEC and ciliated cell lineages

Similar to Conchola et al[33], we also identified a *SCGB3A2+SFTPB+CFTR+* population with a developmental contribution to PNEC and ciliated cells, but also Club cells in later gestational tissues (>GW16). By resolving temporal dynamics, we found a decline in PNEC contribution and concomitant increase in ciliated cell contribution by *SCGB3A2+SFTPB+CFTR+* cells at gestational week 14 (**Fig. 5A**).

We used CellRank to estimate the PNEC or mature ciliated cell fate probability for the *SCGB3A2+SFTPB+CFTR+* cells, showing a decline in PNEC probability and increase in Mature ciliated cell probability with GW (**Fig. 5B**). Spatial transcriptomics show the proximity of both PNEC and ciliated cells with *SCGB3A2+SFTPB+CFTR+* as evident in the demarcated region (red dot) of the scatterpie plots of cell proportions (**Fig. 5C**). Within Visium spots, spatial proximity of PNEC and *SCGB3A2+SFTPB+CFTR+* cells were identified at week 15, while spatial proximity of mature ciliated cells, *SCGB3A2+FOXJ1+* cells, *SCGB3A2+SFTPB+CFTR+* cells were found at week 18 **(Fig. 3C and 5E)**. Together, these results demonstrate a temporal regulation of PNEC and ciliated cell differentiation through *SCGB3A2+SFTPB+CFTR+* cells, supporting the dynamic plasticity of these progenitor cells in the developing lung.

Temporal differences in cell signalling regulates SCGB3A2+SFTPB+CFTR+ epithelial cell fate.

Several new trajectories were observed in mid and late tissues which would suggest that cell fate acquisition is much more dynamic than previously understood. One explanation for these dynamic cell fate changes may reflect changes in the spatial microenvironment of the cell[64] and the various signalling mechanisms (paracrine, autocrine, distant signalling)[65]. To determine the cell autonomous and non-cell autonomous interactions in regulating the change in gene expression and developmental potential of *SCGB3A2+SFTPB+CFTR+* cells, we performed *CellChat*[62]

analysis on our scRNA-seq dataset and identified unique signaling pathways targeting the *SCGB3A2+SFTPB+CFTR+* cells and how they changed across early (GW 10-13), mid (GW 14-16), and late (GW 18-19) fetal lung development (**Extended Data Fig. 6A,B**). Signaling pathways that specifically targeted *SCGB3A2+SFTPB+CFTR+* cells in comparison to other cells and which changed with GW included fibroblast growth factor (FGF), NOTCH and WNT signaling over time. Meanwhile, we observed high levels of NOTCH signaling in early-mid tissues that then decreased in mid-late tissues (**Extended Data Fig. 6A, B**).

We focused our investigation on the FGF signaling pathway as it was observed to have significantly increased (red arrow, **Extended Data Fig. 6A**) over time and known to play a role in branching morphogenesis during lung development[66]. Moreover certain FGF recombinant proteins are also used in many directed differentiation protocols to generate lung epithelia from human iPSC[13,15]. We specifically focused on cell-cell interactions through FGF signaling with *SCGB3A2+SFTPB+CFTR+* cells **(Fig. 5D**). Informed by Visium, we identified cells that were spatially in "close proximity" to *SCGB3A2+SFTPB+CFTR+* cells which included lipofibroblast precursors, *SOX2^{high}CFTR+* cells, PNEC and airway SMC in GW15 lungs; and *SCGB3A2+FOXJ1+* and mature ciliated cells in GW18 lungs (**Fig. 5E**). Further analysis potential signaling partners involved in FGF signaling in *SCGB3A2+SFTPB+CFTR+* target cells (receiver cells of the signal) across time, showed multiple contributions of sender cells that are near the *SCGB3A2+SFTPB+CFTR+* cells and cells that are not spatially close but are sending signals via the FGF pathway (**Fig. 5F**). Interestingly, there were temporal changes in FGF sending cells, but there were also persistent signals from the same senders (ie. Airway fibroblast progenitors) that remained throughout the time points. We do not include PNEC, *SCGB3A2+FOXJ1+*, or Mature Ciliated cells (which are close spatially), as we aim to find the signals interacting with *SCGB3A2+SFTPB+CFTR+* cells which may explain the dynamic change in lineage contributions from these cells.

We then estimated the interaction probability between specific ligand-receptor (L-R) interactions involved in FGF signaling across GWs between *SCGB3A2+SFTPB+CFTR+* cells and FGF signal senders, specifically airway fibroblast progenitors, SMG secretory and airway SMC as they were determined to be cells in close proximity with SCGB3A2+SFTPB+CFTR+ cells, based on Visium spatial transcriptomics (**Fig. 5E, 5G**). We found significantly increased signaling between L-R interactions involving the ligands FGF2 and FGF7 expressed by airway fibroblast progenitors during GW10-13, and we found significantly increased signaling for L-R interactions involving the ligands FGF9, FGF10, and FGF18 expressed in SMG secretory and airway SMC during GW14-16 or GW17-19. Gene expression of the specific FGF ligands and receptors shows elevated expression in the relevant cell types including FGF receptor 2 (*FGFR2*) and 3 (*FGFR3*) in *SCGB3A2+SFTPB+CFTR+* cells **(Extended Data Fig. 6C).** Based on gene expression from the visium platform confirmed high expression of FGFR2 and FGFR3 in regions with high proportions of *SCGB3A2+SFTPB+CFTR+* cells at GW 15 and 18 **(**black box, **Extended Data Fig. 6D).** These results suggest greater contribution of FGF2 and FGF7 signaling by airway fibroblast progenitors during early development, and FGF9, FGF10, and FGF18 signaling by SMG secretory and airway SMC later in development and may explain the temporal switch from PNEC to ciliated cells contributions.

We also assessed Notch signaling in *SCGB3A2+SFTPB+CFTR+* cells and found relatively strong Notch signaling in lung tissues during mid (GW14-16) timepoint **(Extended Data Fig. 6B).** Notch receptors: *NOTCH2* and *NOTCH3* were expressed in multiple cell types including *SCGB3A2+SFTPB+CFTR+* cells and *SCGB3A2+FOXJ1+* cells, but not in PNEC **(Extended Data Fig. 7A).** Whereas NOTCH ligand *JAG1* was expressed in multiple cell types including vascular SMC and *SOX2^{high}CFTR+* cells. High **e**xpression of *NOTCH2* and *NOTCH3* was found in spots with high proportion of *SCGB3A2+SFTPB+CFTR+* cells (black box, **Extended Data Fig. 7B**). Several sources of NOTCH signaling with *SCGB3A2+SFTPB+CFTR+* cells including vascular SMC, and *SOX2^{low}CFTR+* cells, and *SOX2^{high}CFTR+* cells **(Extended Data Fig. 7C**). Interestingly, airway SMC was a source of NOTCH signaling during the "early" stage that was lost in mid/late stages. Increased *JAG1-NOTCH2* and *JAG1-NOTCH3* L-R interactions are also observed in "mid" stage tissues stemming from *SOX2^{high}CFTR+* cells (**Extended Data Fig. 7D**). Overall, our data suggests NOTCH-mediated signaling to *SCGB3A2+SFTPB+CFTR+* during "mid" stage may involve direct interaction with *SOX2^{high}CFTR+* which in turn regulate *SCGB3A2+SFTPB+CFTR+* differentiation during this stage of development.

WNT signaling in *SCGB3A2+SFTPB+CFTR+* cells were also assessed and found to be elevated in early (GW 10-13) and decreased in mid and late stages **(Extended Data Fig. 6B).** WNT receptors *FZD2, FZD3, FZD5, FZD6, FZD7, LRP5, LRP6* were found to be expressed in *SCGB3A2+SFTPB+CFTR+* cells with comparatively higher expression of *FZD2* and *FZD7* in the early stages **(Extended Data Fig. 8A)**. In deconvoluting the spatial expression with Visium, we identified *FZD2, LRP5, LRP6,* and *FZD7* expressed in areas of abundant *SCGB3A2+SFTPB+CFTR+* spots at GW15 whereas *LRP5, FZD3, LRP6,* and *FZD6* were expressed at GW18 **(Extended Data Fig. 8B).** Sources of WNT signalling was assessed in early, mid, late stages to *SCGB3A2+SFTPB+CFTR+* cells where *WNT2* was derived from multiple cell types including airway SMC (only in early stage), lipofibroblast precursors, and airway fibroblast progenitors (**Extended Data Fig. 8C, 8D**). In contrast, while senders of WNT signaling in mid/late stage tissues were like early tissues, SMG secretory cells also became a strong sender in mid/late tissues (**Extended Data Fig. 8D**).

While all of these pathways have previously been described in mammalian lung development[67], future studies will need to confirm their explicit role in specific cell lineage development. Future studies will need to confirm the specific role of these signaling pathways in *SCGB3A2+SFTPB+CFTR+* cell interactions and how the cell interprets the wide array of signals it receives to effect specific functions.

Human pluripotent stem cell (hPSC)-derived fetal lung cultures capture cellular heterogeneity and trajectories found in the native tissue.

Directed differentiation protocols of hPSC aim to capture developmental milestones ensuring robust development of bona fide cell types in cell cultures. However, to do this, differentiation protocols must reflect developmental processes that are observed in the primary tissues. Many differentiation protocols, including for the lung, captures "fetal-like" states but few have benchmarked the developmental stage of these cells to fully understand the stage and potential limitations of the protocols. The human "fetal" stages of tissue development span nearly

9 months of gestation, during which a small batch of early embryonic cells must proliferate, differentiate and migrate to form a complex functional tissue. As the differentiations become more advanced, with the capability to generate hPSC-derived tissues-specific organoids, these models represent an exciting research tool to study fundamental mechanisms of development, especially when access to primary fetal tissues for research is limited. Here, we sought to determine the developmental stage of the cells we considered to be "fetal" lung cells and organoids generated from hPSC using our most recent lung differentiation protocol[13] (**Figure 6A**). We performed scRNA-seq on the hPSC-derived fetal lung cells, considered to contain mostly undifferentiated lung epithelial cells, and fetal organoids, which were subjected to further differentiation. Using batch-balanced nearest neighbors, we integrate the hPSC-derived cells and the primary fetal lung epithelia. The integrated clustering showed significant overlap of hPSC-derived fetal lung cells (green cluster) and organoids (purple cluster) with epithelial cells in the primary tissue (**Fig. 6B, C**). A Pearson correlation coefficient between the hPSC derived cultures and the tissues across gestational timepoints showed a strong correlation (>0.75) to GW13 lung epithelial for hPSC-derived fetal lung cells (Stage 3), and (>0.75) to GW16 to 19 lung epithelia for hPSC-derived organoids (**Fig. 6D**) which represent the next stage of differentiation (Stage 4, **Fig. 6A**). To unbiasedly determine the epithelial cell subtype in the hPSC-derived cultures, we created cell type scores from the top 100 DEG for each cluster identified in the primary epithelial tissue (**Fig. 6E**). Interestingly, proliferating progenitors were the greatest scoring cell type in the hPSC-derived fetal lung cells. This is not surprising as the culture conditions was intended for fetal lung cell growth including retinoic acid, CHIR99021, and FGF7[53]. Other cell types with elevated scores include PNEC, basal, SMG basal and secretory, and stromal-like cells. On the contrary, hPSC-derived fetal lung organoids which represents the next stage following expansion of the fetal lung cells, contained high basal cell scores, along with club cells, PNEC, *SCGB3A2+SFTPB+CFTR+*, SMG basal and secretory cells, and stromal-like cells. The high basal cell score is not surprising as our organoid expansion media contains dual TGFbeta/SMAD signalling inhibitors DMH1 and A83-01 which promotes basal cell expansion[68]. To understand the extent to which these hPSC organoids represent fetal lung epithelial development, we positioned these cells along our previously inferred trajectories. We considered the previously inferred trajectory for the primary fetal epithelium from Budtip progenitors to *SCGB3A2+SFTPB+CFTR+* cells, through early AT2-like cells, *NKX2-1+SOX9+CFTR+* cells, and S$OX2^{high/low}$*CFTR+* cells (**Fig. 6F**). Using the integrated nearest neighbors graph we clustered the integrated cells and considered the clusters with at least 100 cells along the trajectory (**Fig. 6G**). In particular, the hPSC derived cells resided in clusters 1, 9, 7, and 5, with hPSC organoids in all 4 of these clusters and hPSC fetal lung cells only within cluster 1 **(Fig. 6H)**.

Using the average pseudotime of each of these clusters containing hPSC organoid cells, we plotted a heat map of significantly changing genes along the trajectory for these organoid cells. A clear pattern of the change in gene expression emerges, and an analysis of the cell type scores **(Fig. 6I)** indicated that these organoids become increasingly differentiated along this trajectory with the acquisition of specific genes associated various epithelial cell types. In particular, proliferating progenitor and early AT2-like cell type scores were lost with increasing pseudotime and $SOX2^{high/low}$*CFTR+*, *SCGB3A2+SFTPB+CFTR+*, Basal, and club cell type scores increased (**Fig. 6J**).

Overall, we benchmarked our hPSC differentiated fetal cell models to primary late pseudoglandular lung tissues and showed that some fetal lung cell states and trajectories were captured in the differentiation process.

Discussion

Reactivation of developmental mechanisms occur during disease pathogenesis[69](such as pulmonary fibrosis) and tissue repair[70]. Therefore, understanding the plasticity of cells under normal development and the role of the local cellular signalling environment in dictating cell fate and function may provide key insights into congenital lung diseases, chronic disease pathogenesis and the cellular responses to therapies. Here, we created a comprehensive topographic human fetal lung transcriptomic atlas of the developing human fetal lung. Leveraging over 150,000 fetal cells captured, we identify novel cell types/states and inferred developmental trajectories revealing remarkable cellular plasticity within the epithelial compartment. With spatially resolved transcriptomics, we identify putative cell autonomous and non-cell autonomous signalling interactions that dictate cell fate and behaviours within the developing lung. Finally, we show for the first time, the differentiation of hPSC progressing along similar developmental trajectories and giving rise to similar fetal cell types/states as observed in the human fetal lungs. This demonstrates the potential of the hPSC models in elucidating human-specific developmental mechanisms.

The pseudoglandular lung is marked by extensive branching morphogenesis, where the cells must undergo extensive proliferation, proximal-distal patterning, cell migration and differentiation into specialized cell types. A major novel finding in our analysis is the identification of several progenitor cells expressing high levels of CFTR. These cells include the *NKX2-1+SOX9+CFTR+, SOX2^{high}CFTR+, SOX2^{low}CFTR+, and SCGB3A2+SFTPB+CFTR+* cells. The co-expression of CFTR in these progenitor cell types suggest a putative role for CFTR in branching morphogenesis and the formation of specific epithelial cell lineages. In the postnatal lung, mutations in the CFTR gene can cause in cystic fibrosis (CF) disease, a disease that manifests in the airways and impairs lung function and ultimate destruction. The *CFTR* gene encodes for a chloride channel that regulates water and ion transport across the epithelium. The precise role of CFTR in the developing lung is unclear. Understanding the role of CFTR in airway cell development may provide important insight into the early manifestations of CF lung disease and the long-term impact on disease pathogenesis.

Another major finding in our analyses is the uncovering of a broader epithelial cell plasticity and more precise inference of lineage trajectories especially involving the *CFTR+* cells. Proceeding from *NKX2-1+SOX9+CFTR+*, we found a trajectory through *SOX2^{high}CFTR+* and *SOX2^{low}CFTR+* cells to *SCGB3A2+SFTPB+CFTR+* cells. We also found that the *SCGB3A2+SFTPB+CFTR+* cells have the developmental potential for club cells (a secretory cell type), and both PNEC and ciliated cells as has previously shown with *in-vitro* lineage tracing[33]. We were also able to resolve the role of time in the contribution of various epithelial cell subtypes, in which the contribution to cell states/types changed over the course of the 10 weeks of gestation. We demonstrate the multi-lineage plasticity of the epithelium and the remarkably dynamic developmental potential of these cells. Indeed, cellular heterogeneity and high developmental

plasticity has been observed in endothelial lineage development[71] and neutrophil development[72]. Moreover, epithelial plasticity has also been shown to drive the formation of the endoderm during gastrulation[73]. Therefore, it is conceivable that the epithelial cells of the developing lung retained high developmental plasticity that are not observed in developed organs. Notably, this dynamic plasticity was not observed in the stromal compartment. In comparing to the datasets from He et al[9] and Sountoulidis et al.[10], both have found trajectories involving *SCGB3A2+* cells or "proximal progenitor cells" to PNEC respectively, but neither identified the *SCGB3A2+SFTPB+CFTR+* cells specifically to be the source, nor have they identified the various CFTR+ cell subsets that are distinct from other proximal/distal progenitors. Moreover, unlike Conchela et al.[33], we show that contribution to mature ciliated cells from the *SCGB3A2+SFTPB+CFTR+* involves *SCGB3A2+FOXJ1+* cells, which may be an intermediary transient cell state. Overall, we provide key insight into how specific cell lineages are formed in the developing lungs which will inform new cell regeneration strategies for lung diseases.

Developmental processes contributing to cell fate decisions are mediated by precise cell-cell signaling interactions within a cell's microenvironment. While cells may share transcriptomic gene signatures, cell autonomous and non-cell autonomous signalling may dictate how these cells develop. Here we focused on signalling communications between epithelial-epithelial and epithelial-stromal cells however, it does not preclude the contributions of the immune, endothelial, and neural (Schwann) cells that are also co-developed and residing near the former two cell types. Interestingly, *CellChat* analysis informed from spatial Visium data showed temporal change in the signaling pathways targeting the *SCGB3A2+SFTPB+CFTR+* cells, which would suggest that both spatial and temporal effects can influence cell behaviour and potential cell fate decisions. In our study, we confirmed FGF, WNT and NOTCH signalling in fetal lung development. Moreover, we showed how dynamic changes in specific L-R interactions from specific sender cells through the gestational timepoints may regulate *SCGB3A2+SFTPB+CFTR+* cell behaviour and cell fate decisions. Previous studies have demonstrated all three pathways to play a role in lung branching morphogenesis and epithelial differentiation[74]. Mouse studies have suggested distinct signalling pathways driving epithelial specification and branching via Fgf9 and Fgf10, respectively[75]. Moreover, lateral inhibition of Notch signalling increase PNEC differentiation in Hes1-null mice[76]. Similarly, in our data set, we observed a dramatic decrease in PNEC in later gestational lung tissues as NOTCH signalling temporally increased. Future studies will need to determine the precise role of all these signaling pathways (in addition to other pathways) in regulating specific epithelial cell differentiation. Altogether our data highlights the intricate nature of cellular communications within a cell's microenvironment that may contribute to the heterogenous and complex development of the fetal lung epithelium.

An important aspect of our study was the benchmarking of the hPSC-derived fetal lung cells in which the fetal epithelial models generated[13] can capture several of the fetal-specific cell types/states and differentiation trajectories observed in the native tissue. Using single-cell RNA sequencing, we found that differentiated hPSC-derived fetal lung cells, which mostly represents proliferative, uncommitted cells, and hPSC-derived fetal organoids, which represent a later developmental stage, share similar transcriptomic expression to fetal epithelial cells in the pseudoglandular stage (GW13 and GW16-19, respectively). For example, we found cells that

shared a similar transcriptomic profile of proliferating uncommitted epithelial population and AT2-like cells in the primary fetal tissue were mainly represented in hPSC-derived fetal lung cells, whereas cells that shared DEG to *NKX2-1+SOX9+CFTR+, SOX$^{high/low}$CFTR+, SCGB3A2+SFTPB+CFTR+* and basal cells made up the hPSC-derived fetal organoid population. Pseudotime analysis of the hPSC-derived cells showed that the hPSC differentiation captured lineage trajectories originating from proliferating progenitors to *NKX2-1+SOX9+CFTR+*, *SOX2^{high}CFTR+, SOX2^{low}CFTR+* cells and eventually *SCGB3A2+SFTPB+CFTR+* cells, similar to that observed in the primary fetal lung epithelia. Since not all cell types and trajectories were captured, and future studies will need to leverage the predictions of the L-R interactions to modify current differentiation protocols which may help improve the generation of bona fide cell types in vitro. Nonetheless, the significance of this comparison to the fetal lung primary tissues supports the use of hPSC-derived fetal lung epithelial models as a surrogate to study certain aspects of lung development. Moreover, hPSC differentiations are experimentally tractable models and can be used to study broader developmental ranges and origins of diseases, especially since primary tissues may be limited due or restricted.

Our study extensive analysis of the human fetal lungs does have a few limitations. First, while recent publications[9,10] have sequenced earlier fetal lungs (as early as 5PCW), our study protocol precludes the collection of earlier timepoints which could have uncovered additional heterogeneities. Second, our study focused on collecting and analyzing freshly isolated lung tissues in which the tracheas were manually removed and whole lungs immediately processed for single-cell library prep. No cell enrichment for specific populations were performed for the purpose of capturing all cell types. However, this may have inadvertently limited our ability to detect rare cells. Moreover, due to the technical difficulties of accurately discerning "proximal" versus "distal" airways, our data could not resolve regional differences between proximal vs distal specific cell types, as has previously been shown[9]. Despite these technical differences, our data unbiasedly captured many of the cell types/states and developmental trajectories previously observed in recent datasets[9,10,33]. Finally, while our data aimed to prevent over-clustering by using *Clustree* to identify the optimal resolution for sub-clustering, it is possible that this method may not have resolved finer differences in cell states resulting in lower cell types/states identified. Future studies aimed at combining our dataset with proteomics and perturbing gene regulatory networks in functional genomics using hPSC models would provide a powerful resource for understanding the developing human fetal lung.

Overall, our study identified novel cell types/states, trajectories and local interactomes that contributes to the dynamic changes in the early human fetal lung and highlights the complexities of the developing lung. Understanding human fetal lung cell functional diversity and their role in development will improve current differentiation protocols for hPSC to generate better organoid models/bona fide cell types for future therapies for congenital and chronic lung diseases.

References (50 only)

1. Young, M. D. *et al.* Single-cell transcriptomes from human kidneys reveal the cellular identity of renal tumors. *Science* **361**, 594–599 (2018).
2. Baron, M. *et al.* A Single-Cell Transcriptomic Map of the Human and Mouse Pancreas Reveals Inter- and Intra-cell Population Structure. *Cell Syst* **3**, 346-360.e4 (2016).
3. Carraro, G. *et al.* Transcriptional analysis of cystic fibrosis airways at single-cell resolution reveals altered epithelial cell states and composition. *Nat Med* **27**, 806–814 (2021).
4. Travaglini, K. J. *et al.* A molecular cell atlas of the human lung from single-cell RNA sequencing. *Nature* **587**, 619–625 (2020).
5. Vieira Braga, F. A. *et al.* A cellular census of human lungs identifies novel cell states in health and in asthma. *Nat Med* **25**, 1153–1163 (2019).
6. Wang, Z. *et al.* Deciphering cell lineage specification of human lung adenocarcinoma with single-cell RNA sequencing. *Nat Commun* **12**, 6500 (2021).
7. Huang, Y. *et al.* Reconstructing the Developmental Trajectories of Multiple Subtypes in Pulmonary Parenchymal Epithelial Cells by Single-Cell RNA-seq. *Front Genet* **11**, 573429 (2020).
8. Negretti, N. M. *et al.* A single-cell atlas of mouse lung development. *Development* **148**, dev199512 (2021).
9. He, P. *et al.* A human fetal lung cell atlas uncovers proximal-distal gradients of differentiation and key regulators of epithelial fates. *Cell* **185**, 4841-4860.e25 (2022).
10. Sountoulidis, A. *et al.* A topographic atlas defines developmental origins of cell heterogeneity in the human embryonic lung. *Nat Cell Biol* **25**, 351–365 (2023).

11. Cao, S. *et al.* Single-cell RNA sequencing reveals the developmental program underlying proximal–distal patterning of the human lung at the embryonic stage. *Cell Res* **33**, 421–433 (2023).

12. Wong, A. P. *et al.* Directed differentiation of human pluripotent stem cells into mature airway epithelia expressing functional CFTR protein. *Nat Biotechnol* **30**, 876–882 (2012).

13. Ngan, S. Y. *et al.* Stage-Specific Generation of Human Pluripotent Stem Cell Derived Lung Models to Measure CFTR Function. *Curr Protoc* **2**, e341 (2022).

14. Hawkins, F. J. *et al.* Derivation of Airway Basal Stem Cells from Human Pluripotent Stem Cells. *Cell Stem Cell* **28**, 79-95.e8 (2021).

15. Wong, A. P. *et al.* Efficient generation of functional CFTR-expressing airway epithelial cells from human pluripotent stem cells. *Nat Protoc* **10**, 363–381 (2015).

16. Ahmadi, S. *et al.* Phenotypic profiling of CFTR modulators in patient-derived respiratory epithelia. *NPJ Genom Med* **2**, (2017).

17. Jiang, J. X. *et al.* A new platform for high-throughput therapy testing on iPSC-derived lung progenitor cells from cystic fibrosis patients. *Stem Cell Reports* **16**, 2825–2837 (2021).

18. Farrell, S., Mani, M. & Goyal, S. Inferring single-cell transcriptomic dynamics with structured latent gene expression dynamics. 2022.08.22.504858 Preprint at https://doi.org/10.1101/2022.08.22.504858 (2022).

19. Street, K. *et al.* Slingshot: cell lineage and pseudotime inference for single-cell transcriptomics. *BMC Genomics* **19**, 477 (2018).

20. Zappia, L. & Oshlack, A. Clustering trees: a visualization for evaluating clusterings at multiple resolutions. *GigaScience* **7**, giy083 (2018).

21. Tata, A. *et al.* Myoepithelial Cells of Submucosal Glands Can Function as Reserve Stem Cells to Regenerate Airways after Injury. *Cell Stem Cell* **22**, 668-683.e6 (2018).

22. Park, J. *et al.* The Tcf21 lineage constitutes the lung lipofibroblast population. *Am J Physiol Lung Cell Mol Physiol* **316**, L872–L885 (2019).

23. Liu, X. *et al.* Categorization of lung mesenchymal cells in development and fibrosis. *iScience* **24**, 102551 (2021).

24. McGowan, S. E. & Torday, J. S. The pulmonary lipofibroblast (lipid interstitial cell) and its contributions to alveolar development. *Annu Rev Physiol* **59**, 43–62 (1997).

25. Naim, H. M. & Tyms, A. S. Thymidine kinase activity in mouse embryo fibroblast cells infected with murine cytomegalovirus. *Biochem Biophys Res Commun* **99**, 855–863 (1981).

26. Penke, L. R. *et al.* FOXM1 is a critical driver of lung fibroblast activation and fibrogenesis. *J Clin Invest* **128**, 2389–2405 (2018).

27. Ward, C. *et al.* Fine-Tuning Mybl2 Is Required for Proper Mesenchymal-to-Epithelial Transition during Somatic Reprogramming. *Cell Rep* **24**, 1496-1511.e8 (2018).

28. Gill, S. E. *et al.* Tissue inhibitor of metalloproteinases-3 moderates the proinflammatory status of macrophages. *Am J Respir Cell Mol Biol* **49**, 768–777 (2013).

29. Simovic Markovic, B. *et al.* Galectin-3 Plays an Important Pro-inflammatory Role in the Induction Phase of Acute Colitis by Promoting Activation of NLRP3 Inflammasome and Production of IL-1β in Macrophages. *J Crohns Colitis* **10**, 593–606 (2016).

30. Tao, L., Huang, G., Song, H., Chen, Y. & Chen, L. Cancer associated fibroblasts: An essential role in the tumor microenvironment. *Oncol Lett* **14**, 2611–2620 (2017).

31. Li, J. *et al.* TMEM158 promotes the proliferation and migration of glioma cells via STAT3 signaling in glioblastomas. *Cancer Gene Ther* **29**, 1117–1129 (2022).

32. Danopoulos, S. *et al.* Human lung branching morphogenesis is orchestrated by the spatiotemporal distribution of ACTA2, SOX2, and SOX9. *American Journal of Physiology-Lung Cellular and Molecular Physiology* **314**, L144–L149 (2018).

33. Conchola, A. S. *et al.* Regionally distinct progenitor cells in the lower airway give rise to neuroendocrine and multiciliated cells in the developing human lung. *Proc Natl Acad Sci U S A* **120**, e2210113120 (2023).

34. Rawlins, E. L., Clark, C. P., Xue, Y. & Hogan, B. L. M. The Id2+ distal tip lung epithelium contains individual multipotent embryonic progenitor cells. *Development* **136**, 3741–3745 (2009).

35. Warburton, D. YAP and TAZ in Lung Development: The Timing Is Important. *Am J Respir Cell Mol Biol* **62**, 141–142 (2020).

36. Zhang, K. *et al.* mTORC1 signaling facilitates differential stem cell differentiation to shape the developing murine lung and is associated with mitochondrial capacity. *Nat Commun* **13**, 7252 (2022).

37. Fernandes-Silva, H., Araújo-Silva, H., Correia-Pinto, J. & Moura, R. S. Retinoic Acid: A Key Regulator of Lung Development. *Biomolecules* **10**, 152 (2020).

38. Meyerholz, D. K. *et al.* Lack of cystic fibrosis transmembrane conductance regulator disrupts fetal airway development in pigs. *Lab Invest* **98**, 825–838 (2018).

39. Castel, D. *et al.* Dynamic binding of RBPJ is determined by Notch signaling status. *Genes Dev* **27**, 1059–1071 (2013).

40. Wan, H. *et al.* Compensatory roles of Foxa1 and Foxa2 during lung morphogenesis. *J Biol Chem* **280**, 13809–13816 (2005).

41. Hawkins, F. *et al.* Prospective isolation of NKX2-1-expressing human lung progenitors derived from pluripotent stem cells. *J Clin Invest* **127**, 2277–2294 (2017).

42. Chung, M.-I., Bujnis, M., Barkauskas, C. E., Kobayashi, Y. & Hogan, B. L. M. Niche-mediated BMP/SMAD signaling regulates lung alveolar stem cell proliferation and differentiation. *Development* **145**, dev163014 (2018).

43. Rockich, B. E. *et al.* Sox9 plays multiple roles in the lung epithelium during branching morphogenesis. *Proc Natl Acad Sci U S A* **110**, E4456-4464 (2013).

44. Gotoh, S. *et al.* Generation of alveolar epithelial spheroids via isolated progenitor cells from human pluripotent stem cells. *Stem Cell Reports* **3**, 394–403 (2014).

45. Khetchoumian, K. *et al.* Pituitary cell translation and secretory capacities are enhanced cell autonomously by the transcription factor Creb3l2. *Nat Commun* **10**, 3960 (2019).

46. Shi, N., Zhang, J. & Chen, S.-Y. Runx2, a novel regulator for goblet cell differentiation and asthma development. *FASEB J* **31**, 412–420 (2017).

47. Reynolds, S., Reynolds, P., Pryhuber, G., Finder, J. & Stripp, B. Secretoglobins SCGB3A1 and SCGB3A2 define secretory cell subsets in mouse and human airways. *American journal of respiratory and critical care medicine* **166**, 1498–509 (2003).

48. Plasschaert, L. W. *et al.* A single cell atlas of the tracheal epithelium reveals the CFTR-rich pulmonary ionocyte. *Nature* **560**, 377–381 (2018).

49. Wallmeier, J. *et al.* Mutations in TP73 cause impaired mucociliary clearance and lissencephaly. *Am J Hum Genet* **108**, 1318–1329 (2021).

50. Campbell, E. P., Quigley, I. K. & Kintner, C. Foxn4 promotes gene expression required for the formation of multiple motile cilia. *Development* **143**, 4654–4664 (2016).

51. Ruiz García, S. *et al.* Novel dynamics of human mucociliary differentiation revealed by single-cell RNA sequencing of nasal epithelial cultures. *Development* **146**, dev177428 (2019).

52. Kappen, C. Hox genes in the lung. *Am J Respir Cell Mol Biol* **15**, 156–162 (1996).

53. Miller, A. J. *et al.* In Vitro Induction and In Vivo Engraftment of Lung Bud Tip Progenitor Cells Derived from Human Pluripotent Stem Cells. *Stem Cell Reports* **10**, 101–119 (2017).

54. Sun, D. *et al.* SOX9 maintains human foetal lung tip progenitor state by enhancing WNT and RTK signalling. *EMBO J* **41**, e111338 (2022).

55. Zhou, B. *et al.* Comprehensive epigenomic profiling of human alveolar epithelial differentiation identifies key epigenetic states and transcription factor co-regulatory networks for maintenance of distal lung identity. *BMC Genomics* **22**, 906 (2021).

56. Zhang, Z. *et al.* Transcription factor Etv5 is essential for the maintenance of alveolar type II cells. *Proc Natl Acad Sci U S A* **114**, 3903–3908 (2017).

57. Thul, P. J. & Lindskog, C. The human protein atlas: A spatial map of the human proteome. *Protein Sci* **27**, 233–244 (2018).

58. Valcourt, U., Thuault, S., Pardali, K., Heldin, C.-H. & Moustakas, A. Functional role of Meox2 during the epithelial cytostatic response to TGF-beta. *Mol Oncol* **1**, 55–71 (2007).

59. Rankin, S. A. *et al.* A Retinoic Acid-Hedgehog Cascade Coordinates Mesoderm-Inducing Signals and Endoderm Competence during Lung Specification. *Cell Rep* **16**, 66–78 (2016).

60. Borromeo, M. D. *et al.* ASCL1 and NEUROD1 Reveal Heterogeneity in Pulmonary Neuroendocrine Tumors and Regulate Distinct Genetic Programs. *Cell Rep* **16**, 1259–1272 (2016).

61. Lange, M. *et al.* CellRank for directed single-cell fate mapping. *Nat Methods* **19**, 159–170 (2022).

62. Whitsett, J. A. Airway Epithelial Differentiation and Mucociliary Clearance. *Ann Am Thorac Soc* **15**, S143–S148 (2018).

63. Montoro, D. T. *et al.* A revised airway epithelial hierarchy includes CFTR-expressing ionocytes. *Nature* **560**, 319–324 (2018).

64. Kholodenko, B. N. Cell-signalling dynamics in time and space. *Nat Rev Mol Cell Biol* **7**, 165–176 (2006).

65. Müller, P. & Schier, A. F. Extracellular movement of signaling molecules. *Dev Cell* **21**, 145–158 (2011).

66. Danopoulos, S., Shiosaki, J. & Al Alam, D. FGF Signaling in Lung Development and Disease: Human Versus Mouse. *Front Genet* **10**, 170 (2019).

67. Herriges, M. & Morrisey, E. E. Lung development: orchestrating the generation and regeneration of a complex organ. *Development* **141**, 502–513 (2014).

68. Mou, H. *et al.* Dual SMAD Signaling Inhibition Enables Long-Term Expansion of Diverse Epithelial Basal Cells. *Cell Stem Cell* **19**, 217–231 (2016).

69. Froidure, A. *et al.* Chaotic activation of developmental signalling pathways drives idiopathic pulmonary fibrosis. *Eur Respir Rev* **29**, 190140 (2020).

70. Hogan, B. L. M. *et al.* Repair and regeneration of the respiratory system: complexity, plasticity, and mechanisms of lung stem cell function. *Cell Stem Cell* **15**, 123–138 (2014).

71. Paik, D. T. *et al.* Single-Cell RNA Sequencing Unveils Unique Transcriptomic Signatures of Organ-Specific Endothelial Cells. *Circulation* **142**, 1848–1862 (2020).

72. Salcher, S. *et al.* High-resolution single-cell atlas reveals diversity and plasticity of tissue-resident neutrophils in non-small cell lung cancer. *Cancer Cell* **40**, 1503-1520.e8 (2022).

73. Scheibner, K. *et al.* Epithelial cell plasticity drives endoderm formation during gastrulation. *Nat Cell Biol* **23**, 692–703 (2021).

74. Nikolić, M. Z., Sun, D. & Rawlins, E. L. Human lung development: recent progress and new challenges. *Development* **145**, dev163485 (2018).

75. Yin, Y. & Ornitz, D. M. FGF9 and FGF10 activate distinct signaling pathways to direct lung epithelial specification and branching. *Sci Signal* **13**, eaay4353 (2020).

76. Ito, T. *et al.* Basic helix-loop-helix transcription factors regulate the neuroendocrine differentiation of fetal mouse pulmonary epithelium. *Development* **127**, 3913–3921 (2000).

Main Figures

Fig 1: Overview of the single-cell RNA sequencing dataset from 19 fetal lung tissues.

A: Biological sex of the lungs was determined by *SRY, XIST*, and *DDX3Y* expression.

B: UMAP visualization of the dataset highlighting the main cell types: stromal, epithelial, endothelial, immune, and schwann cells.

C: Gene expression heatmap of the top 5 differentially expressed genes in each cluster.

D: UMAP projection of all 58 cell types/states identified within the integrated dataset. The number of clusters were determined by *Clustree*.

E: UMAP projection of the integrated fetal lung datasets annotated by gestational week (GW).

F: UMAP projection of two recently published fetal lung datasets (He et al. and Sountoulidis et al.) overlayed onto our dataset as determined by single-cell reference mapping (Seurat).

G: Proportion of cell types shared and unique to our dataset.

Fig 2: Characterization of the stromal cell compartment identifies lipofibroblast and lipofibroblast progenitors as main cell type in the developing fetal lungs.

A: UMAP visualization of the fetal stromal cell subtypes.

B: Proportion of stromal cell subtypes across gestational week.

C: Gene expression heatmap of the top 5 differentially expressed genes in each cluster.

D: Dotplot of the top differentially expressed transcription factors (TF) genes based on regulon specificity score (RSS) via *SCENIC.*

E: LatentVelo analysis revealing inferred cell state trajectories projected onto the UMAP.

F: Partition-based graph abstraction (PAGA) plot identified lineage trajectories informed by LatentVelo velocities.

G: Slingshot trajectory analysis with a root at Cycling fibroblasts identifies a trajectory to Lipofiblasts. Trajectory heatmap plot shows the progression of cell types along the trajectory, and the change in significantly varying genes.

H: Slingshot trajectory analysis with a root at Cycling fibroblasts identifies a trajectory to Airway fibroblast progenitors.

Fig 3: Heterogenous and novel cell types identified in the developing fetal lung epithelium.

A: UMAP visualization of the fetal epithelial subtypes.

B: Gene expression heatmap of the top 3 differentially expressed genes in each cluster.

C: Correlation between RCTD weights for Visium spots. Showing the colocalization of specific celltypes within the same Visium spots. Hierarchical clustering shows groups of frequently colocalized cells.

D: Spatial transcriptomic analysis (10X Visium) shows areas of localization of budtip progenitors, *PTEN+STAT3+* cells, early AT2-like cells, *NKX2-1+SOX9+CFTR+* cells, $SOX^{low}CFTR+$ cells, $SOX2^{high}CFTR+$ cells in GW15 fetal lung tissue. Location of Visium spots with highest RCTD weights (green-yellow hue) for the major immune cell types. High magnification of H&E staining shows a specific region where there is an abundant number of the specific cell subtype (red dot). Pie chart (insert) shows the proportion of the cells in the specific region (red dot).

E: Given Visium spots with RCTD proportion for a specific cell type above 0.1, we plot the average proportion of spatially close epithelial cell types.

F: Immunofluorescent staining shows the localization of SOX2, SOX9, CFTR, SCGB3A2, and SFTPB positive cells in the fetal lungs (GW15 tissue). Inset is the negative (no primary, secondary antibodies only) controls. DAPI marks all nuclei. Dashed lines and arrows demarcate areas of SOX2 low and high expression, respectively.

Fig 4. RNA velocity analysis reveals dynamic epithelial cell trajectories varying across gestational ages.

A: LatentVelo analysis revealing inferred cell state trajectories projected onto the UMAP.

B: Terminal states identified by using velocities with CellRank,shown on the UMAP.

C: Partition-based graph abstraction (PAGA) analysis reveals multiple connections with the fetal epithelia.

D: LatentVelo PAGA is subset into Early (GW10-13), Mid (GW14-16), and Late (GW17-19). The weakening of PNEC transitions were observed, and the emergence of transitions to ciliated cells with increasing GW.

E: Based on the PAGA, the early trajectories to PNEC from Stromal-like cells 1 and *SCGB3A2+SFTPB+CFTR+* cells are analyzed with Slingshot. Trajectory heatmaps show the progression of cell types (colored bar) and significantly varying genes along the trajectory.

F: Mid timepoint Slingshot trajectories highlighting the emergence of mature ciliated cells from Stromal-like cells 1 and *SCGB3A2+SFTPB+CFTR+* cells are shown.

G: Based on PAGA, basal cells contribute to late club and PNEC cells. Slingshot trajectories show the development of PNEC cells from basal cells, and the development of Club cells from basal and *SCGB3A2+SFTPB+CFTR+* cells.

Fig 5. Regulation of TP cells differentiation and cell communication.

A: Heatmap showing the gene-normalized expression of the top 20 differentially expressed genes for the PNEC and mature ciliated cells within the *SCGB3A2+SFTPB+CFTR+* cells versus Gestational Week.

B: CellRank mature ciliated and PNEC fate probabilities for *SCGB3A2+SFTPB+CFTR+* cells versus Gestational Week.

C: Spatial transcriptomic analysis (10X Visium) shows areas of localization of *SCGB3A2+SFTPB+CFTR+* cells, PNEC, mature ciliated cells in GW15 fetal lung tissue. Location of Visium spots with highest RCTD weights are demarcated in green-yellow hue. High magnification of H&E staining shows a specific region where there is an abundant number of the specific cell subtype (asterisk). Pie chart (insert) shows the proportion of the cells in the specific region (red dot).

D: FGF signalling interaction probabilities towards *SCGB3A2+SFTPB+CFTR+* cells from specific cell types.

E: Given Visium spots with RCTD proportion for *SCGB3A2+SFTPB+CFTR+* cells above 0.1, we plot the average proportion of spatially close cell types.

F: FGF signalling interactions towards *SCGB3A2+SFTPB+CFTR+* cells subset to cell types in close proximity **(Fig. 5E**). Size of the incoming arrows indicate strength of signalling.

G: Significant ligand-receptor (L-R) interactions towards *SCGB3A2+SFTPB+CFTR+* cells for the FGF pathway, subset to signalling cell types in proximity. Both color and point size indicate interaction probability. Top row shows L-R interactions significantly increased early. Bottom row shows interactions significantly increased mid/late. All significance tests use $p < 0.01$.

Fig 6: hPSC-derived lung models recapitulate trajectories towards basal and CFTR-expressing cells from the fetal lung epithelia.

A: Stage-specific differentiation of hPSC towards mature proximal airway epithelia.

B: Integrated UMAP projection of hPSC-derived fetal lung cells and organoid integrated with primary fetal lung epithelia.

C: Integrated UMAP projection of hPSC-derived fetal lung cells and organoids cells.

D: Pearson correlation between hPSC-derived fetal lung models and primary-derived fetal lung epithelia using the top 50 DEG for each gestational week.

E: Proportion of primary and hPSC derived fetal models within clusters 1, 5, 7, and 9.

F: Cell type scores based on the top 100 DEGs from the primary fetal epithelia reveal high proliferating progenitor scores in the hPSC fetal lung cells and high basal scores in the hPSC organoids.

G: Previously derived primary fetal trajectory from Budtip progenitors to *SCGB3A2+SFTPB+CFTR+* cells through Early AT2-like, *NKX2-1+SOX9+CFTR+*, and *SOX2*^{high}*CFTR+* cells on the integrated UMAP. Color shows increasing pseudotime.

H: Integrated clustering of the primary fetal and hPSC derived cells focused on clusters 1, 5, 7 and 9 which contains hPSC organoids and primary fetal cells.

I: Trajectory heat map showing the change in gene expression of hPSC organoids within these clusters, ordered by increasing average pseudotime of the primary fetal cells within each cluster.

J: Celltype score for the hPSC organoids within the ordered clusters.

K: Primary fetal and hPSC derived cells along the inferred trajetory. hPSC fetal lung cells resemble the early part of the trajectory, and hPSC organoids the later.

Extended Data Figures

Extended Data Fig 1: Analytical pipeline and characterization of the human fetal lung.
A: Computational pipeline for single-cell RNA sequencing analysis.
B: *Clustree* analysis to determine the number of cell clusters. We selected the resolution in which the number of cell clusters would not yield "overlapping" subpopulations.
C: Proportion of the major cell types across GW.
D: Integrated UMAP projections of all three datasets of human fetal lungs (He et al., 2022, Sountoulidis et al., 2022, and our dataset).
E: *MapQuery* analysis using our dataset as the reference map to identify cell subtypes common in adult lung tissues. Adult lung datatset was obtained from Travaglini et al. 2020.
F: *MapQuery* analysis using our dataset as the reference map to identify cell subtypes common in mouse embryonic lung tissues. Mouse lung datatset was obtained from Negretti et al. 2021.

Extended Data Fig 2: Spatial transcriptomic of the fetal stromal cell compartment.
H&E staining shows the gross morphological features of the lung tissue. Visium spots with highest RCTD weights (green-yellow hue) for the major immune cell types. Top row: Representative GW15 fetal lung tissue. Bottom row: Representative GW18 fetal lung tissue.

Extended Data Fig 3: Characterization of the developing fetal lung epithelium.
A: Proportion of the epithelial cell subtypes across GW.
B: Dotplot for SOX2, SOX9 and CFTR to determine proximal, distal and cell expressing high levels of CFTR, respectively.
C: Dotplot of the top differentially expressed transcription factors (TF) genes based on regulon specificity score (RSS) via *SCENIC.*
D: Immunofluorescent staining THBS1, expressed in *PTEN+STAT3+* cells. Inset is the negative (no primary, secondary antibodies only) controls. DAPI marks all nuclei.
E: Immunofluorescent staining deltaN P63 (basal cell), SCGB3A2 (secretory), and FOXJ1 (ciliated cell) in GW15 fetal lung epithelium. Inset is the negative (no primary, secondary antibodies only) controls. DAPI marks all nuclei.

Extended Data Fig 4: Spatial determination of epithelial subtypes in the fetal lungs and comparisons with published fetal lung datasets.
A: Spatial transcriptomic analysis (10X Visium) shows areas of localization of budtip progenitors, *PTEN+STAT3+* cells, early AT2-like cells, *NKX2-1+SOX9+CFTR+* cells, $SOX2^{low}CFTR+$ cells, $SOX2^{high}CFTR+$ cells in GW18 fetal lung tissue. Location of Visium spots with highest RCTD weights (green-yellow hue) for the major immune cell types. High magnification of H&E staining shows a specific region where there is an abundant number of the specific cell subtype (red dot). Pie chart (insert) shows the proportion of the cells in the specific region (red dot).
B: Immunofluorescent staining acetylated alpha tubulin (cilia on multiciliated cells) and ASCL1 (PNEC) in GW15 fetal lung epithelium. Inset is the negative (no primary, secondary antibodies only) controls. DAPI marks all nuclei.

C: UMAP feature plots for *GRP* and *GHRL* demarcating two PNEC populations also identified in previous datasets.
D: *MapQuery* analysis using our dataset as the reference map to identify shared cell subtypes with the dataset from Peng et al., 2022.
E: *MapQuery* analysis using our dataset as the reference map to identify shared cell subtypes with the dataset from Sountoulidis et al., 2022.

Extended Data Fig 5: Validation of LatentVelo trajectories and analysis of distal trajectories.
A: Palantir was used to infer pseudotimes, starting with a root at GW10 budtip cells. CellRank was used to infer a transition matrix between cells, and transitions were projected onto the UMAP. Results largely agree with LatentVelo, except for a clearer distinction of the terminal budtip state. The same terminal states at PNEC, Mature ciliated cells, and later GW budtip cells were observed.
B: Mature ciliated cell and PNEC fate probabilities vs Palantir pseudotime. *SCGB3A2+SFTPB+CFTR+* cells were situated in the middle near 0.5, indicating their involvement in both lineages.
C: Fate probabilities for the 3 terminal states. Fate probabilities for both the Stromal-like cells 1 and club cells, and *SCGB3A+SFTPB+CFTR+* and *SOX2+CFTR+* cells were elevated for the Mature ciliated and PNEC terminal states, as was also found with LatentVelo.
D: Analysis of the budtip terminal state with Slingshot. A root was selected at early GW cells. Slingshot identified a bifurcation going towards the late GW budtip terminal state, or towards Early AT2-like cells and *NKX2-1+SOX9+CFTR+* cells. The Slingshot pseudotimes were correlated with GW.

Extended Data Fig 6: FGF cell signaling networks from senders to *SCGB3A2+SFTPB+CFTR+* cells.
A: Relative information flow of signalling towards *SCGB3A2+SFTPB+CFTR+* cells for Early (GW10-13), Mid (GW14-16), and Late (GW17-19). Information flow is calculated as the sum of all cell interaction probabilities towards *SCGB3A2+SFTPB+CFTR+* cells.
B: Overview of signaling pathways strength towards *SCGB3A2+SFTPB+CFTR+* cells in early (GW 10-13), mid (GW 14-16), late (GW 17-19)
C. Expression of FGF ligands and receptors in specific epithelial and stromal subset of cells from scRNAseq grouped by early (GW 10-13), mid (GW 14-16), and late (GW17-19) stages.
D. Expression of FGF ligands and receptors near *SCGB3A2+SFTPB+CFTR+* cells (black box on H&E staining) using Visium spatial transcriptomics.

Extended Data Fig 7: Notch signalling from senders to *SCGB3A2+SFTPB+CFTR+* cells.
A. Expression of Notch ligands and receptors in specific epithelial and stromal subset of cells from scRNAseq grouped by early (GW 10-13), mid (GW 14-16), and late (GW17-19) stages.
B. Expression of Notch ligands and receptors near *SCGB3A2+SFTPB+CFTR+* cells (black box on H&E staining) using Visium spatial transcriptomics.

C. Chord diagrams demonstrating epithelial and stromal cell types that are senders of Notch signaling to *SCGB3A2+SFTPB+CFTR+* cells in early, mid, late stages.
D. Ligand-receptor (L-R) plot showcasing specific NOTCH ligand-receptor interactions enriched in early vs mid/late from airway SMC, lipofibroblast precursors, airway fibroblast progenitors, and SMG secretory cells to *SCGB3A2+SFTPB+CFTR+* cells. Top show interactions significantly increased early, bottom shows interactions significantly increased mid/late. All tests use $p < 0.01$.

Extended Data Fig 8: WNT signalling from senders to *SCGB3A2+SFTPB+CFTR+* cells.
A. Expression of WNT ligands and receptors in specific epithelial and stromal subset of cells from scRNAseq grouped by early (GW 10-13), mid (GW 14-16), and late (GW17-19) stages.
B. Expression of WNT ligands and receptors near *SCGB3A2+SFTPB+CFTR+* cells (black box on H&E staining) using Visium spatial transcriptomics.
C. Chord diagrams demonstrating epithelial and stromal cell types that are senders of WNT signaling to *SCGB3A2+SFTPB+CFTR+* cells in early, mid, late stages.
D. Ligand-receptor (L-R) plot showcasing specific WNT ligand-receptor interactions enriched in early vs mid/late from airway SMC, lipofibroblast precursors, airway fibroblast progenitors, and SMG secretory cells to *SCGB3A2+SFTPB+CFTR+* cells. Top show interactions significantly increased early, bottom shows interactions significantly increased mid/late. All tests use $p < 0.01$.

Supplementary Tables

Table 1: Detailed list of fetal lung tissue samples sequenced

Sample ID (Gestational week_+ day)	Sex	# of sequenced cells	# of genes	Filtered # of cells	% change of cells
GW_10_1	Female	13852	27559	12412	0.103956107
GW_10_2	Male	5937	17271	5515	0.07107967
GW_11_1	Male	4923	16935	4629	0.059719683
GW_12_3	Male	10689	17067	10277	0.038544298
GW_13_4	Male	3748	16573	3588	0.042689434
GW_13_6	Male	13464	17276	13054	0.030451575
GW_14_3	Male	3916	16255	3748	0.042900919
GW_15_5	Female	15444	18067	8168	0.471121471
GW_15_5_1	Female	8849	17214	13347	-0.508306023
GW_16_1	Male	6425	16835	5636	0.122801556
GW_16_2	Female	7687	16415	7380	0.039937557
GW_16_5	Female	5524	24481	4566	0.173425054
GW_18	Male	10505	16700	10477	0.002665397
GW_18_1	Male	12109	16855	10876	0.101825089
GW_18_2	Female	6330	16223	6060	0.042654028
*GW_18_1A	Male	7621	17182	6920	0.091982679
*GW_18_1B	Male	6341	17061	5888	0.071439836
GW_19_0	Male	10565	17664	9764	0.075816375
GW_19_2	Female	6847	16970	6107	0.10807653
GW_19_4	Male	9480	25027	8286	0.125949367
Total count	**7 Female 12 Male**	**170256**		**156698**	

*Same gestational lung tissue. “A” and “B” indicates different regions (lower and upper regions) of the lung tissue sampled for sequencing.

Table 2: List of cell type markers top differentially expressed genes.
Please see attached excel file.

Table 3: Percentages of cell subtypes

CELL TYPE	GW 10	GW 11	GW 12	GW 13	GW 14	GW 15	GW 16	GW 18	GW 19
Erythrocyte like EC 1	17.78	11.15	16.83	28.59	32.08	10.53	16.65	13.96	17.80
KIT CA4 endothelial cells	22.78	19.59	20.04	12.30	10.74	19.77	11.24	21.85	19.33
Erythrocyte like EC 2	15.08	8.45	14.63	13.48	18.29	10.30	16.94	11.55	13.21
Intermediate lymphatic EC	0.87	2.36	0.80	5.19	3.05	4.74	10.60	4.64	1.70
Venous EC	7.30	8.11	12.22	4.59	4.21	12.78	9.58	9.65	10.65
Aerocyte	10.40	16.22	12.42	8.74	13.93	10.38	5.75	4.86	8.99
gCap	7.70	10.14	8.22	7.56	8.56	7.22	5.19	6.60	8.49
Arterial EC	6.43	6.08	7.01	4.00	3.05	3.61	7.24	6.81	7.32
Lymphatic EC	4.21	13.51	2.40	12.44	3.77	17.44	14.30	17.32	8.55
Cycling early capillaries	7.46	4.39	5.41	3.11	2.32	3.23	2.51	2.75	3.96
Common lymphoid progenitor (CLP)	29.55	15.15	19.68	11.04	15.88	26.00	7.83	11.62	18.59
Monocyte 1	2.64	3.03	11.17	18.00	9.44	3.56	11.06	9.53	8.88
aM1 cells	2.11	10.61	3.19	10.14	5.58	13.28	8.01	6.91	8.16
aM like cells	4.22	7.58	12.77	4.24	18.88	4.18	23.45	5.46	6.02
IL7R+ T cells	10.82	9.09	5.32	1.97	2.58	9.25	5.26	7.31	8.46
Proliferating macrophage/monocyte cells	17.68	24.24	12.23	10.44	6.44	11.89	3.20	3.98	6.52
aM2 cells	9.23	1.52	6.38	7.72	9.87	10.26	5.15	4.69	6.90
B cells	0.53	0.00	0.00	0.76	3.43	0.46	3.34	10.88	3.70
Macrophage	8.71	7.58	4.26	6.35	6.01	7.78	3.01	5.44	4.75
Monocyte/macrophage precursors	7.65	7.58	12.23	11.80	9.44	1.60	12.35	3.61	3.87
CD1C+ DC	1.06	1.52	4.79	5.45	6.87	2.98	4.70	4.50	9.34
Monocyte 2	0.53	4.55	3.72	5.60	1.72	1.01	1.76	9.45	1.60
Plasma cell	1.06	1.52	1.06	1.06	0.00	0.92	1.36	6.57	2.65
Cycling B cells	0.00	0.00	0.00	1.66	0.86	0.34	3.12	4.42	1.51
Cycling lymphocytes	2.90	4.55	1.60	1.97	0.86	2.30	2.32	1.50	2.15
Immature DP leukocytes	0.53	1.52	1.06	0.61	0.00	2.34	1.47	1.50	2.82
FLT3+ preDC	0.79	0.00	0.00	1.06	0.86	1.38	2.06	1.47	2.36
pDC	0.00		0.53	0.15	1.29	0.46	0.55	1.16	1.72
Lipofibroblasts	23.55	39.04	30.08	31.25	32.75	30.83	29.17	34.25	27.22
Lipofibroblast precursors	24.15	17.69	30.16	19.73	22.97	25.81	36.44	32.64	31.93

Uncommitted cells	17.74	8.25	10.82	20.73	13.97	12.03	7.84	10.37	9.01
Early fibroblasts	12.24	12.40	9.82	9.80	10.46	6.35	5.88	4.00	3.89
Airway fibroblast progenitors	4.35	4.62	4.69	4.44	4.22	4.96	8.11	6.81	11.69
Airway SMC	4.78	5.65	3.89	3.53	3.63	9.45	4.47	4.80	7.99
Cycling fibroblasts	10.12	9.88	7.53	7.63	6.55	4.91	4.65	2.60	2.62
Vascular SMC	2.56	2.35	2.20	2.03	4.89	4.56	2.90	2.97	4.86
Chondrocyte	0.05	0.00	0.17	0.18	0.43	0.74	0.20	1.10	0.54
Unknown stromal cells	0.46	0.13	0.64	0.69	0.12	0.38	0.34	0.46	0.25
Budtip progenitors	4.90	12.73	5.75	4.96	7.39	9.17	9.33	7.04	20.69
Stromal-like cells 1	15.19	10.91	11.51	26.59	17.12	4.03	9.27	15.52	12.33
Mature ciliated	0.17	0.00	0.00	0.40	7.78	17.31	7.36	10.38	7.21
Early AT2-like	6.02	4.85	5.75	6.75	3.50	7.30	9.21	7.20	10.10
Proliferating progenitors	10.86	3.64	4.66	3.37	2.33	7.42	4.84	3.81	5.21
SOX2lowCFTR+	7.48	12.12	9.32	6.94	4.28	6.45	4.67	5.14	5.85
SOX2highCFTR+	14.35	16.36	13.42	11.90	1.95	4.69	3.41	4.29	4.36
PTEN+STAT3+ cells	5.80	9.70	12.88	6.94	7.39	2.16	7.78	10.75	6.05
SCGB3A2+SFTPB+ CFTR+	6.47	3.64	5.21	3.77	3.11	7.37	3.05	4.08	3.04
Ciliated precursor cells	0.00	0.00	0.27	1.79	25.68	3.21	16.03	5.35	2.39
NKX2-1+SOX9+CFTR+	2.03	1.82	3.56	1.79	1.56	3.60	4.13	5.99	7.32
PNEC	12.04	14.55	12.33	6.55	10.12	3.86	2.33	1.01	1.29
SCGB3A2+FOXJ1+	0.11	0.61	0.00	0.20	2.72	7.58	4.19	3.34	2.20
Stromal-like cells 2	2.08	0.00	2.74	2.98	1.56	2.62	4.31	5.56	5.74
SMG basal	6.92	0.00	0.00	0.00	0.00	6.10	0.00	0.00	0.00
Club	3.83	6.67	5.21	8.93	1.56	1.68	2.93	5.08	2.31
NRGN+ cells	1.58	2.42	7.12	5.16	1.17	2.31	4.61	4.29	2.56
SMG secretory	0.17	0.00	0.27	0.99	0.78	2.33	1.85	0.90	0.08
Basal	0.00	0.00	0.00	0.00	0.00	0.82	0.72	0.26	1.27

Table 4: List of primary and secondary antibodies.

Primary Antibodies	Host	Supplier	Cat. no.	Dilution	Assay
Acetyl-alpha tubulin	Mouse	Invitrogen	322700	1:200	IF
ASCL1	Rabbit	Abcam	Ab74056	1:200	IF
CFTR	Mouse	Millipore	MAB1660	1:70	IF
CGRP	Mouse	Sigma	C9487	1:100	IF
Delta NP63	Rabbit	Biolegend	619002	1:200	IF
FOXJ1	Rabbit	Sigma	HPA005714	1:175	IF
SOX2	Goat	R&D	AF2018	1:300	IF
SOX9	Goat	R&D	AF3075	1:600	IF
SCGB1A1	Rat	R&D	MAB4218	1:50	IF
SCGB3A2	Goat	Santa Cruz	sc-48320	1:50	IF
PGP9.5	Mouse	Abcam	ab20559	1:100	IF
ProSPB	Rabbit	Abcam	ab40876	1:50	IF
ProSPC	Rabbit	Abcam	ab40879	1:100	IF
THBS1	Mouse	LS Bio	LS-C87	1:50	IF
TTF1	Rabbit	Abcam	ab76013	1:200	IF

Secondary Antibodies	Host	Supplier	Cat. no.	Dilution	Assay
Anti-rabbit IgG (H+L) Alexa Fluor 488	Donkey	Invitrogen	A21206	1:500	IF
Anti-mouse IgG (H+L) Alexa Fluor 546	Donkey	Invitrogen	A10036	1:500	IF
Anti-goat IgG (H+L) Alexa Fluor 647	Donkey	Invitrogen	A21447	1:500	IF
Anti-mouse IgG (H+L) Alexa Fluor 488	Donkey	Invitrogen	A21202	1:500	IF
Anti-goat IgG (H+L) Alexa Fluor 546	Donkey	Invitrogen	A11056	1:500	IF
Anti-Rabbit IgG (H&L) Alexa Fluor 647	Donkey	Abcam	ab150075	1:500	IF
Anti-rat IgG (H+L) Alexa Fluor 555	Donkey	Invitrogen	A48270	1:500	IF
Anti-rabbit IgG (H+L) Alexa Fluor 546	Donkey	Invitrogen	A10040	1:500	IF

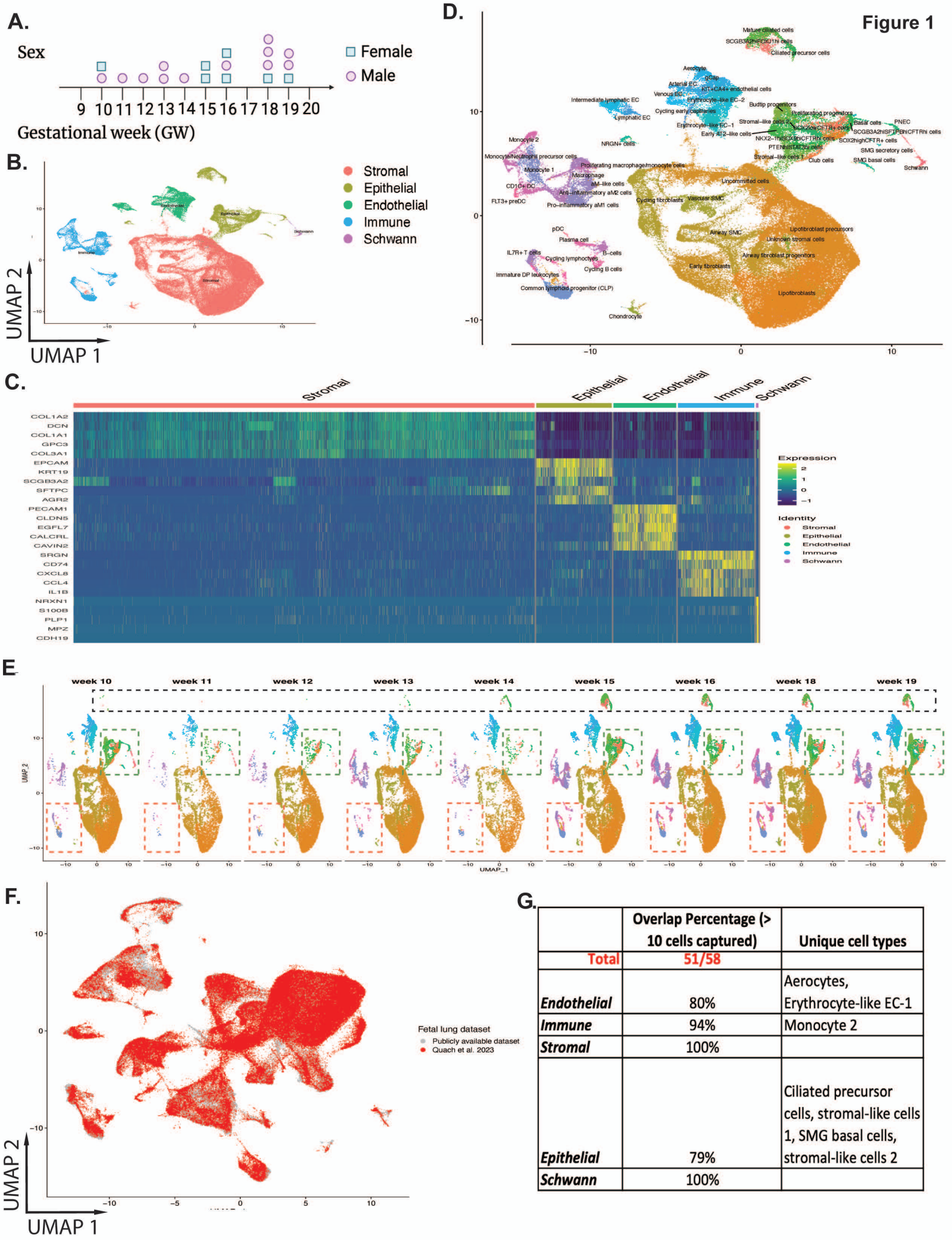

	Overlap Percentage (> 10 cells captured)	Unique cell types
Total	51/58	
Endothelial	80%	Aerocytes, Erythrocyte-like EC-1
Immune	94%	Monocyte 2
Stromal	100%	
Epithelial	79%	Ciliated precursor cells, stromal-like cells 1, SMG basal cells, stromal-like cells 2
Schwann	100%	

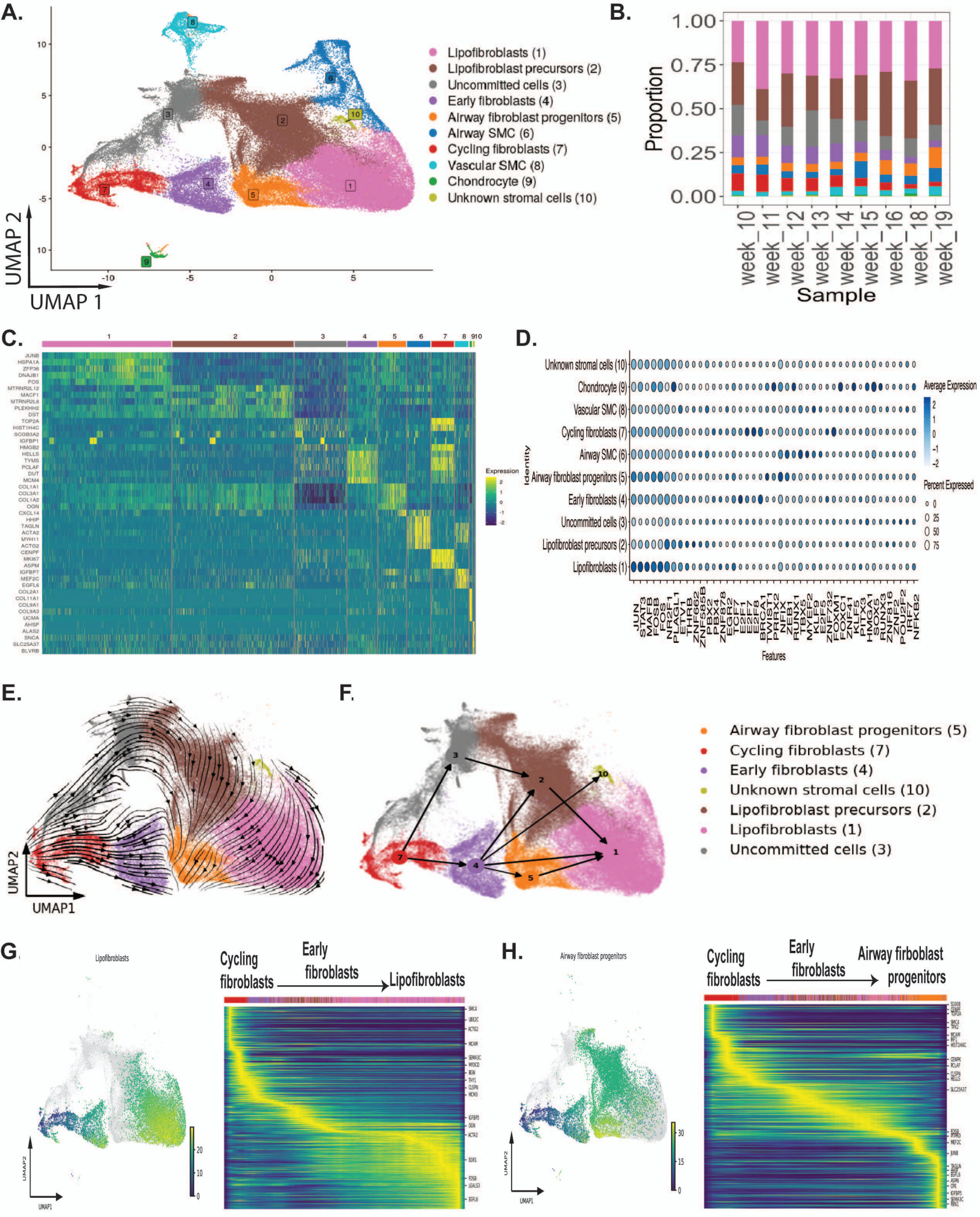
A.
Lipofibroblasts (1)
Lipofibroblast precursors (2)
Uncommitted cells (3)
Early fibroblasts (4)
Airway fibroblast progenitors (5)
Airway SMC (6)
Cycling fibroblasts (7)
Vascular SMC (8)
Chondrocyte (9)
Unknown stromal cells (10)
UMAP 2
UMAP 1
B.
Proportion
Sample
week_10
week_11
week_12
week_13
week_14
week_15
week_16
week_18
week_19
C.
Expression
D.
Unknown stromal cells (10)
Chondrocyte (9)
Vascular SMC (8)
Cycling fibroblasts (7)
Airway SMC (6)
Airway fibroblast progenitors (5)
Early fibroblasts (4)
Uncommitted cells (3)
Lipofibroblast precursors (2)
Lipofibroblasts (1)
Identity
Features
Average Expression
Percent Expressed
E.
UMAP2
UMAP1
F.
Airway fibroblast progenitors (5)
Cycling fibroblasts (7)
Early fibroblasts (4)
Unknown stromal cells (10)
Lipofibroblast precursors (2)
Lipofibroblasts (1)
Uncommitted cells (3)
G.
Lipofibroblasts
Cycling fibroblasts
Early fibroblasts
Lipofibroblasts
H.
Airway fibroblast progenitors
Cycling fibroblasts
Early fibroblasts
Airway firboblast progenitors

Figure 3

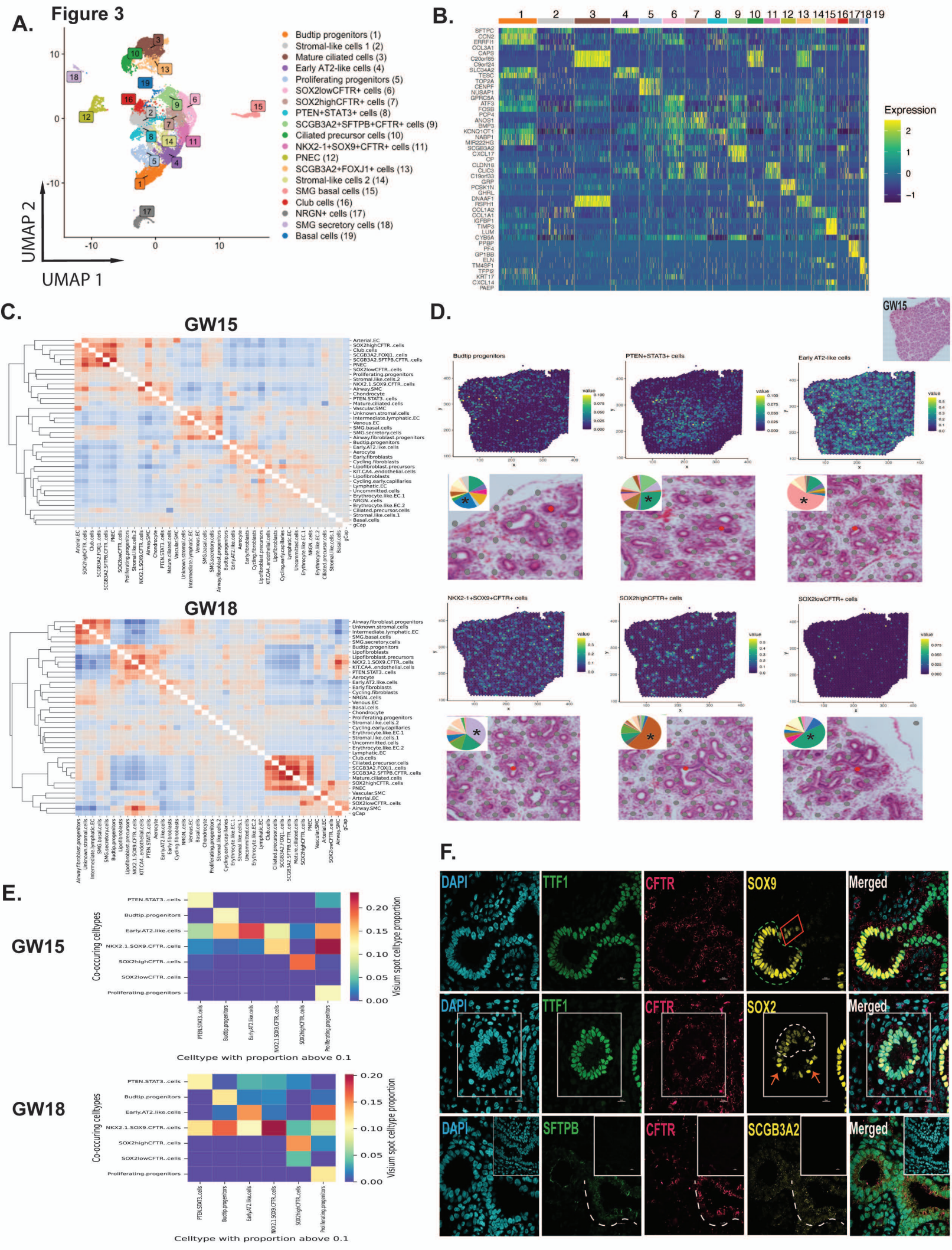
A.
Budtip progenitors (1)
Stromal-like cells 1 (2)
Mature ciliated cells (3)
Early AT2-like cells (4)
Proliferating progenitors (5)
SOX2lowCFTR+ cells (6)
SOX2highCFTR+ cells (7)
PTEN+STAT3+ cells (8)
SCGB3A2+SFTPB+CFTR+ cells (9)
Ciliated precursor cells (10)
NKX2-1+SOX9+CFTR+ cells (11)
PNEC (12)
SCGB3A2+FOXJ1+ cells (13)
Stromal-like cells 2 (14)
SMG basal cells (15)
Club cells (16)
NRGN+ cells (17)
SMG secretory cells (18)
Basal cells (19)
UMAP 1
UMAP 2
B.
Expression
C.
GW15
GW18
D.
GW15
Budtip progenitors
PTEN+STAT3+ cells
Early AT2-like cells
NKX2-1+SOX9+CFTR+ cells
SOX2highCFTR+ cells
SOX2lowCFTR+ cells
E.
GW15
GW18
Co-occuring celltypes
Visium spot celltype proportion
Celltype with proportion above 0.1
F.
DAPI
TTF1
CFTR
SOX9
Merged
SOX2
SFTPB
SCGB3A2

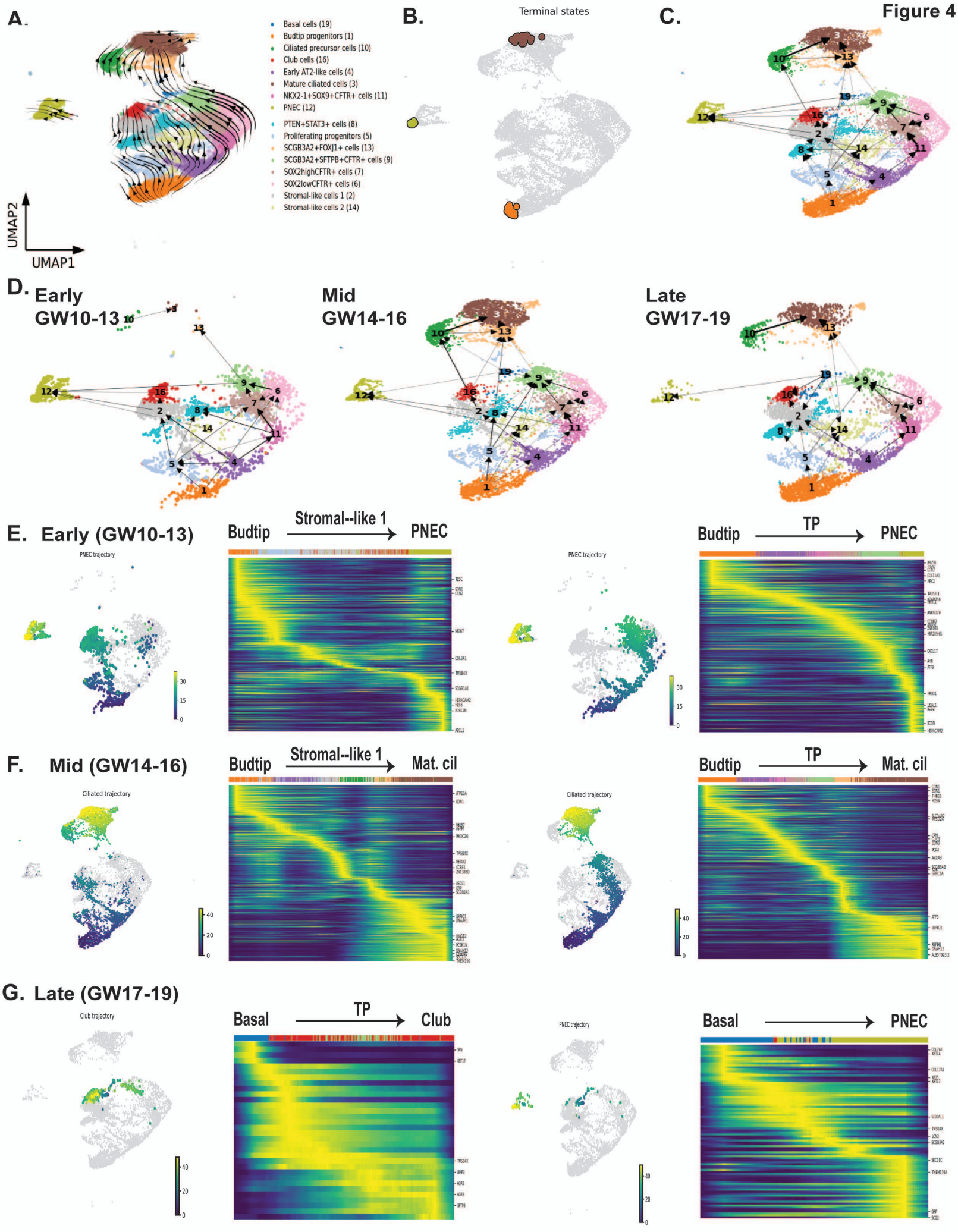
Figure 4
A.
Basal cells (19)
Budtip progenitors (1)
Ciliated precursor cells (10)
Club cells (16)
Early AT2-like cells (4)
Mature ciliated cells (3)
NKX2-1+SOX9+CFTR+ cells (11)
PNEC (12)
PTEN+STAT3+ cells (8)
Proliferating progenitors (5)
SCGB3A2+FOXJ1+ cells (13)
SCGB3A2+SFTPB+CFTR+ cells (9)
SOX2highCFTR+ cells (7)
SOX2lowCFTR+ cells (6)
Stromal-like cells 1 (2)
Stromal-like cells 2 (14)
UMAP2
UMAP1
B.
Terminal states
C.
D.
Early
GW10-13
Mid
GW14-16
Late
GW17-19
E. Early (GW10-13)
PNEC trajectory
Budtip
Stromal--like 1
PNEC
TP
F. Mid (GW14-16)
Ciliated trajectory
Mat. cil
G. Late (GW17-19)
Club trajectory
Basal
Club

Figure 5

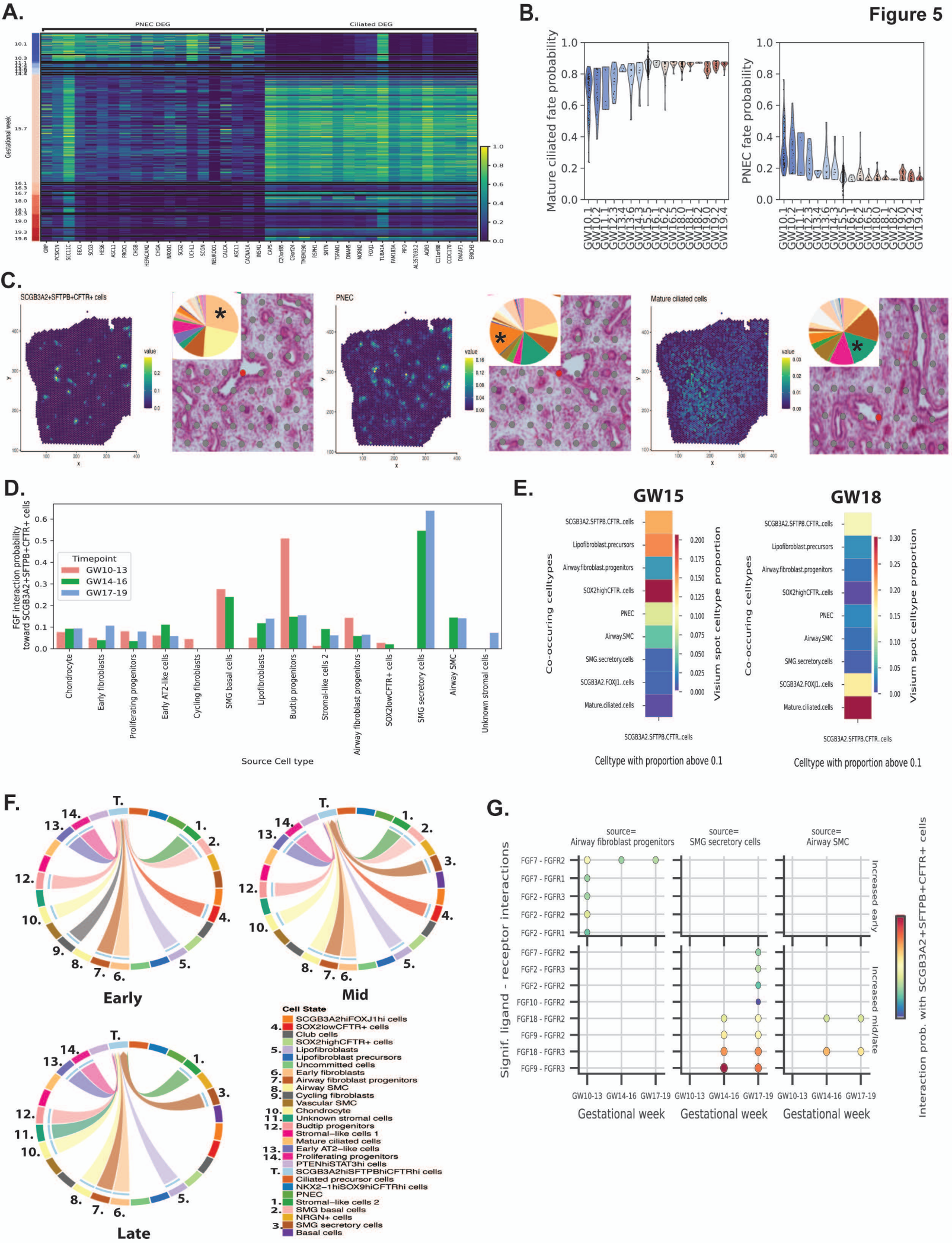
A.
PNEC DEG
Ciliated DEG
Gestational week
B.
Mature ciliated fate probability
PNEC fate probability
C.
SCGB3A2+SFTPB+CFTR+ cells
PNEC
Mature ciliated cells
value
D.
FGF interaction probability toward SCGB3A2+SFTPB+CFTR+ cells
Timepoint
GW10-13
GW14-16
GW17-19
Chondrocyte
Early fibroblasts
Proliferating progenitors
Early AT2-like cells
Cycling fibroblasts
SMG basal cells
Lipofibroblasts
Budtip progenitors
Stromal-like cells 2
Airway fibroblast progenitors
SOX2lowCFTR+ cells
SMG secretory cells
Airway SMC
Unknown stromal cells
Source Cell type
E.
GW15
GW18
Co-occuring celltypes
Visium spot celltype proportion
SCGB3A2.SFTPB.CFTR..cells
Lipofibroblast.precursors
Airway.fibroblast.progenitors
SOX2highCFTR..cells
PNEC
Airway.SMC
SMG.secretory.cells
SCGB3A2.FOXJ1..cells
Mature.ciliated.cells
Celltype with proportion above 0.1
F.
Early
Mid
Late
Cell State
SCGB3A2hiFOXJ1hi cells
SOX2lowCFTR+ cells
Club cells
SOX2highCFTR+ cells
Lipofibroblasts
Lipofibroblast precursors
Uncommitted cells
Early fibroblasts
Airway fibroblast progenitors
Airway SMC
Cycling fibroblasts
Vascular SMC
Chondrocyte
Unknown stromal cells
Budtip progenitors
Stromal–like cells 1
Mature ciliated cells
Early AT2–like cells
Proliferating progenitors
PTENhiSTAT3hi cells
SCGB3A2hiSFTPBhiCFTRhi cells
Ciliated precursor cells
NKX2–1hiSOX9hiCFTRhi cells
PNEC
Stromal–like cells 2
SMG basal cells
NRGN+ cells
SMG secretory cells
Basal cells
G.
source= Airway fibroblast progenitors
source= SMG secretory cells
source= Airway SMC
Signif. ligand - receptor interactions
Increased early
Increased mid/late
Gestational week
Interaction prob. with SCGB3A2+SFTPB+CFTR+ cells

Figure 6

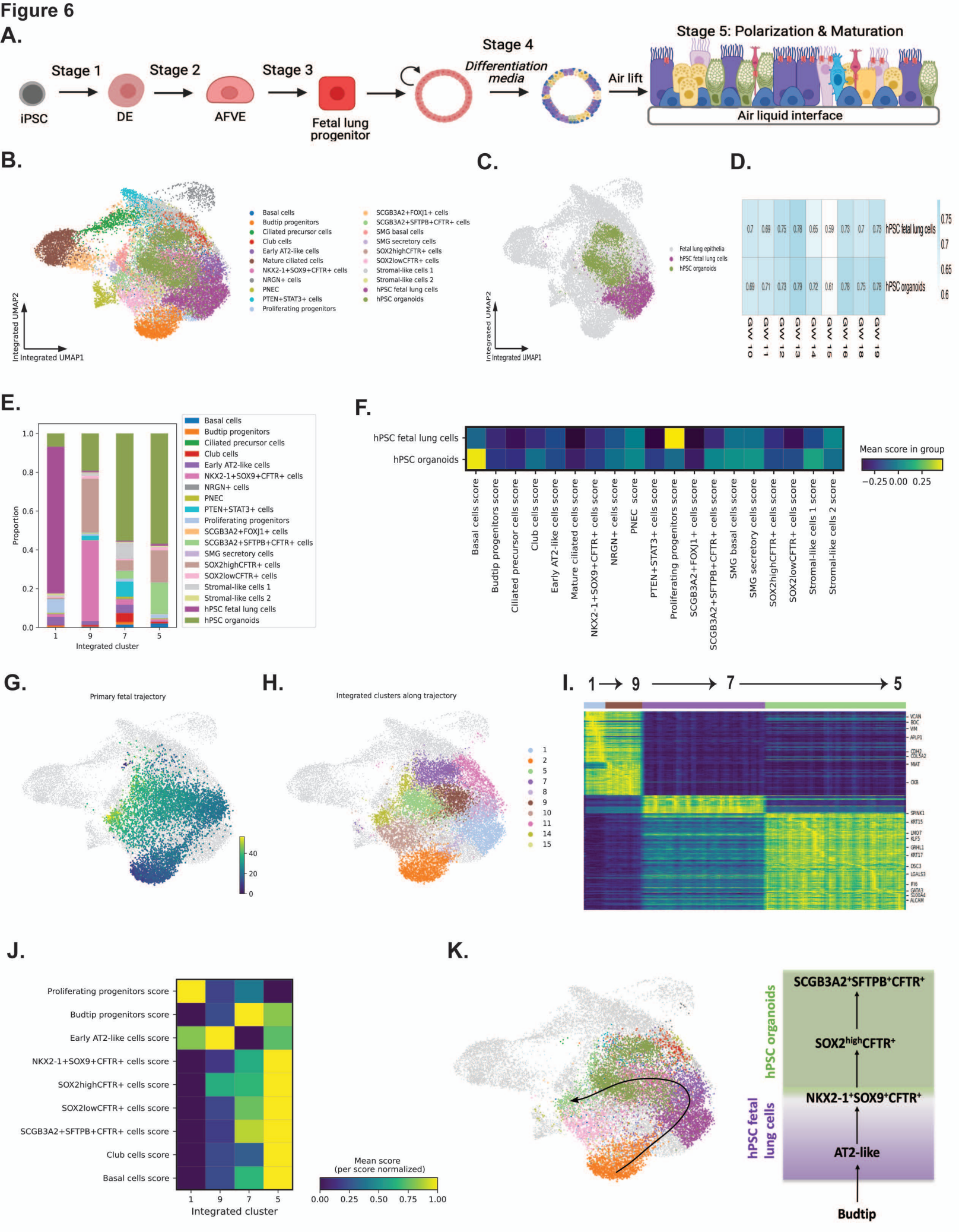
A.
Stage 1
Stage 2
Stage 3
Stage 4
Differentiation media
Stage 5: Polarization & Maturation
Air lift
iPSC
DE
AFVE
Fetal lung progenitor
Air liquid interface
B.
Basal cells
Budtip progenitors
Ciliated precursor cells
Club cells
Early AT2-like cells
Mature ciliated cells
NKX2-1+SOX9+CFTR+ cells
NRGN+ cells
PNEC
PTEN+STAT3+ cells
Proliferating progenitors
SCGB3A2+FOXJ1+ cells
SCGB3A2+SFTPB+CFTR+ cells
SMG basal cells
SMG secretory cells
SOX2highCFTR+ cells
SOX2lowCFTR+ cells
Stromal-like cells 1
Stromal-like cells 2
hPSC fetal lung cells
hPSC organoids
Integrated UMAP1
Integrated UMAP2
C.
Fetal lung epithelia
hPSC fetal lung cells
hPSC organoids
Integrated UMAP1
Integrated UMAP2
D.
hPSC fetal lung cells
hPSC organoids
GW 10
GW 11
GW 12
GW 13
GW 14
GW 15
GW 16
GW 18
GW 19
E.
Proportion
Integrated cluster
F.
hPSC fetal lung cells
hPSC organoids
Basal cells score
Budtip progenitors score
Ciliated precursor cells score
Club cells score
Early AT2-like cells score
Mature ciliated cells score
NKX2-1+SOX9+CFTR+ cells score
NRGN+ cells score
PNEC score
PTEN+STAT3+ cells score
Proliferating progenitors score
SCGB3A2+FOXJ1+ cells score
SCGB3A2+SFTPB+CFTR+ cells score
SMG basal cells score
SMG secretory cells score
SOX2highCFTR+ cells score
SOX2lowCFTR+ cells score
Stromal-like cells 1 score
Stromal-like cells 2 score
Mean score in group
G.
Primary fetal trajectory
H.
Integrated clusters along trajectory
I.
1 → 9 → 7 → 5
J.
Proliferating progenitors score
Budtip progenitors score
Early AT2-like cells score
NKX2-1+SOX9+CFTR+ cells score
SOX2highCFTR+ cells score
SOX2lowCFTR+ cells score
SCGB3A2+SFTPB+CFTR+ cells score
Club cells score
Basal cells score
Integrated cluster
Mean score (per score normalized)
K.
hPSC organoids
hPSC fetal lung cells
SCGB3A2+SFTPB+CFTR+
SOX2highCFTR+
NKX2-1+SOX9+CFTR+
AT2-like
Budtip

Extended Data Fig 1

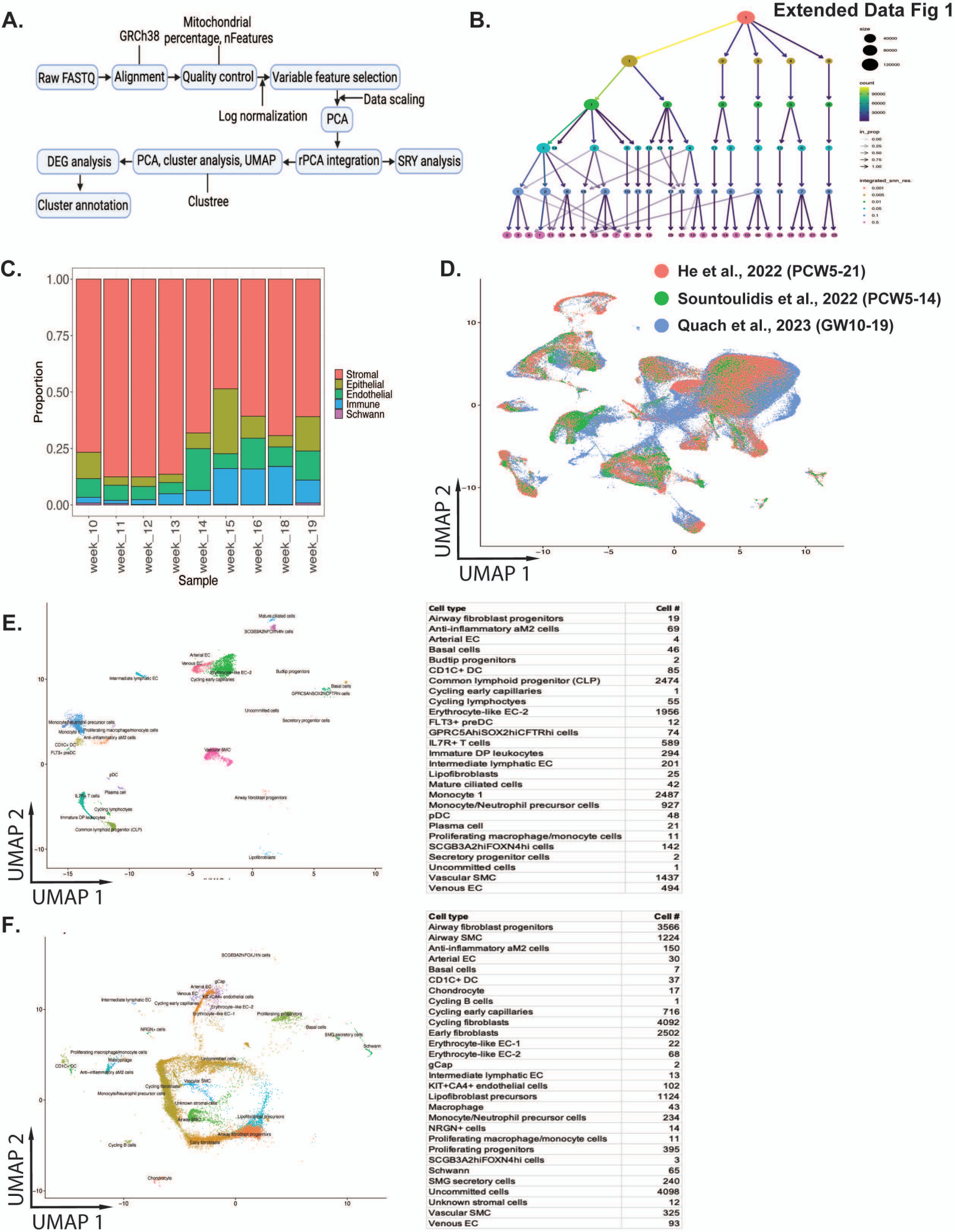

Cell type	Cell #
Airway fibroblast progenitors	19
Anti-inflammatory aM2 cells	69
Arterial EC	4
Basal cells	46
Budtip progenitors	2
CD1C+ DC	85
Common lymphoid progenitor (CLP)	2474
Cycling early capillaries	1
Cycling lymphoctyes	55
Erythrocyte-like EC-2	1956
FLT3+ preDC	12
GPRC5AhiSOX2hiCFTRhi cells	74
IL7R+ T cells	589
Immature DP leukocytes	294
Intermediate lymphatic EC	201
Lipofibroblasts	25
Mature ciliated cells	42
Monocyte 1	2487
Monocyte/Neutrophil precursor cells	927
pDC	48
Plasma cell	21
Proliferating macrophage/monocyte cells	11
SCGB3A2hiFOXN4hi cells	142
Secretory progenitor cells	2
Uncommitted cells	1
Vascular SMC	1437
Venous EC	494

Cell type	Cell #
Airway fibroblast progenitors	3566
Airway SMC	1224
Anti-inflammatory aM2 cells	150
Arterial EC	30
Basal cells	7
CD1C+ DC	37
Chondrocyte	17
Cycling B cells	1
Cycling early capillaries	716
Cycling fibroblasts	4092
Early fibroblasts	2502
Erythrocyte-like EC-1	22
Erythrocyte-like EC-2	68
gCap	2
Intermediate lymphatic EC	13
KIT+CA4+ endothelial cells	102
Lipofibroblast precursors	1124
Macrophage	43
Monocyte/Neutrophil precursor cells	234
NRGN+ cells	14
Proliferating macrophage/monocyte cells	11
Proliferating progenitors	395
SCGB3A2hiFOXN4hi cells	3
Schwann	65
SMG secretory cells	240
Uncommitted cells	4098
Unknown stromal cells	12
Vascular SMC	325
Venous EC	93

Extended Data Fig 2

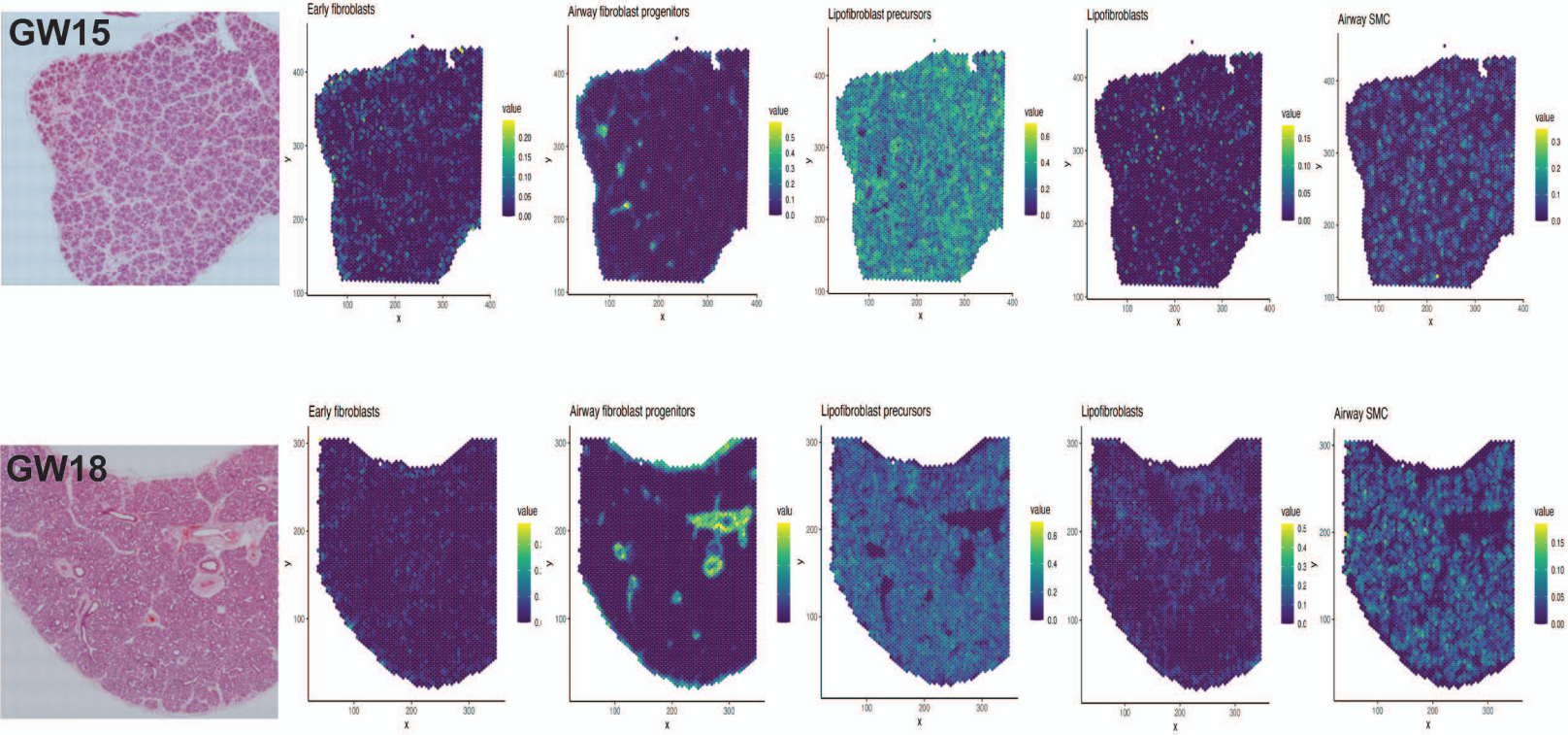

Extended Data Fig 3

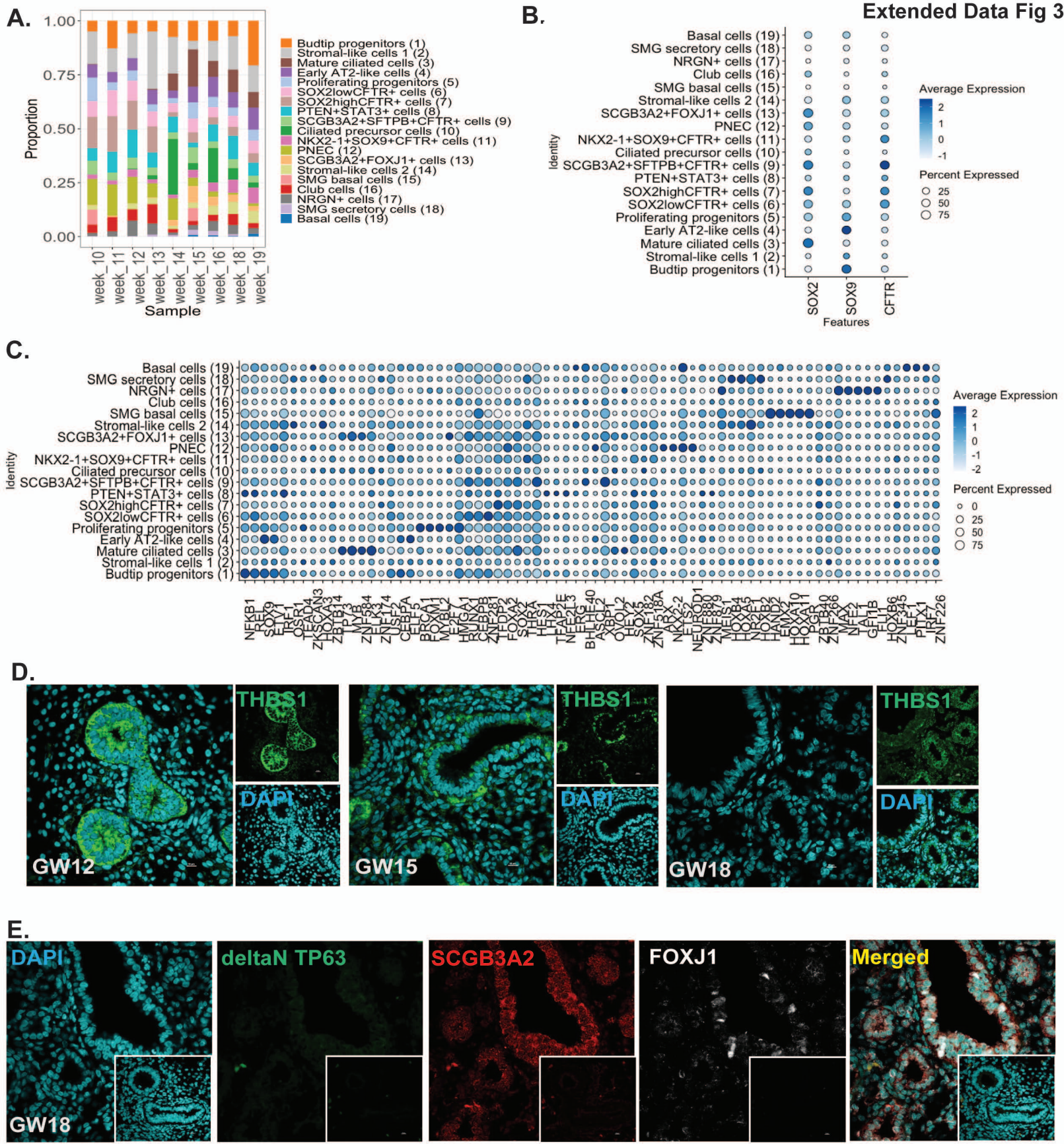

A.

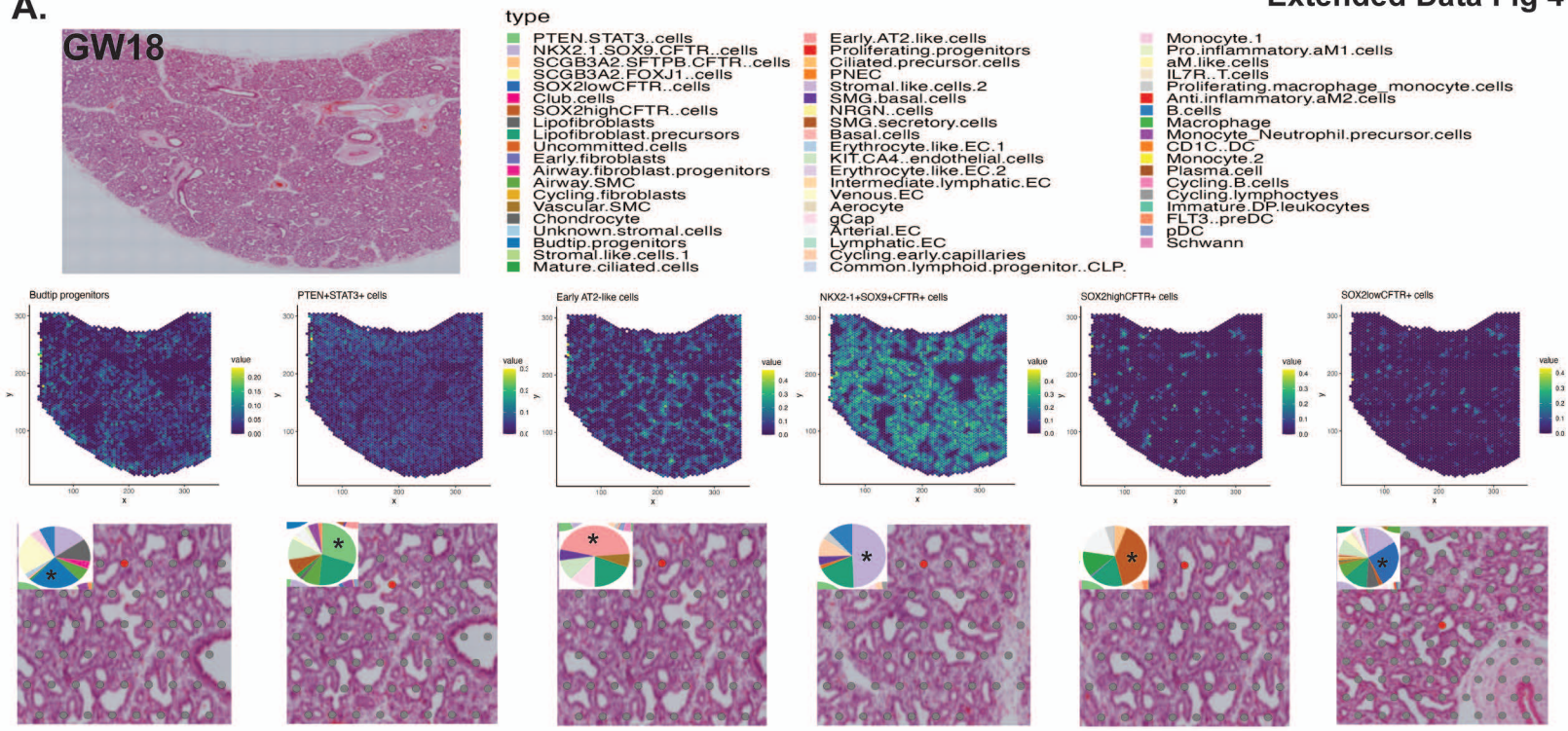

B.

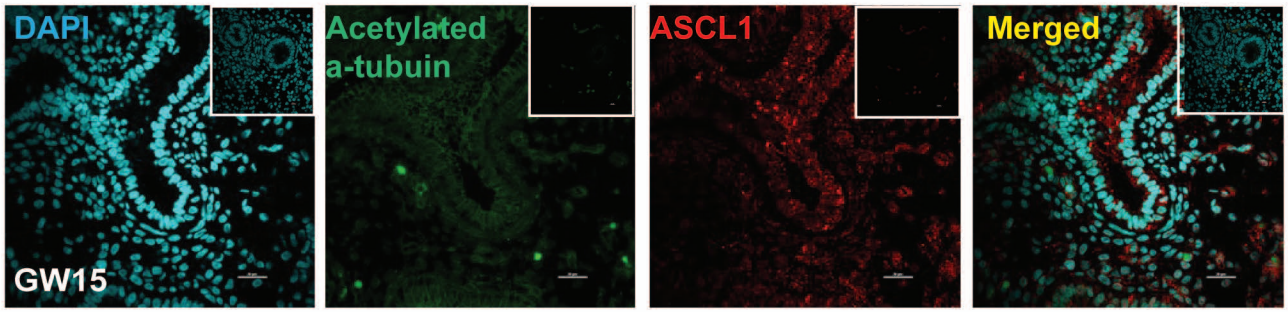

C.

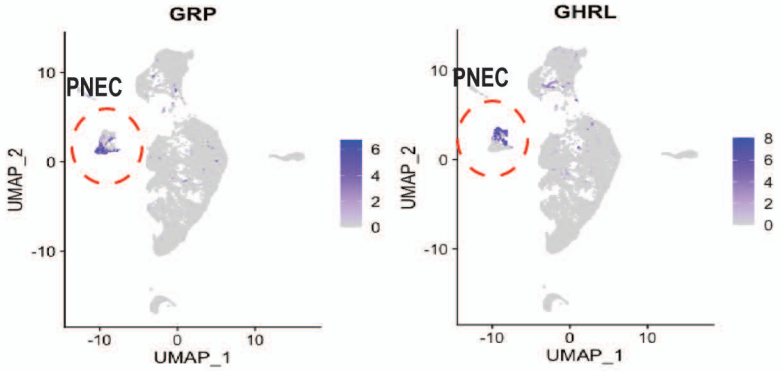

D.

Query to Peng et al (2023)

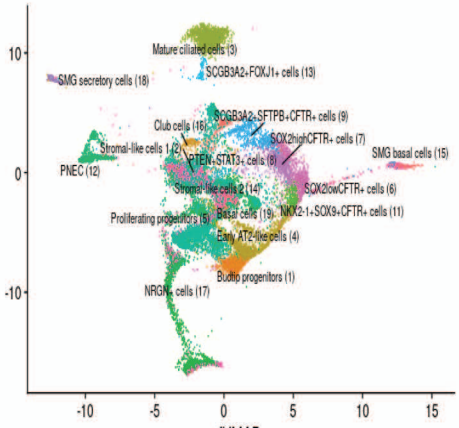

Common cell subtype	Freq
Basal cells (19)	1181
Budtip progenitors (1)	1988
Club cells (16)	309
Early AT2-like cells (4)	1791
Mature ciliated cells (3)	1552
NKX2-1+SOX9+CFTR+ cells (11)	401
NRGN+ cells (17)	4337
PNEC (12)	764
Proliferating progenitors (5)	17385
PTEN+STAT3+ cells (8)	62
SCGB3A2+FOXJ1+ cells (13)	88
SCGB3A2+SFTPB+CFTR+ cells (9)	571
SMG basal cells (15)	5761
SMG secretory cells (18)	283
SOX2highCFTR+ cells (7)	685
SOX2lowCFTR+ cells (6)	923
Stromal-like cells 1 (2)	19353
Stromal-like cells 2 (14)	14318
Cell not found in Peng et al dataset	
Ciliated precursor cell (10)	

E.

Query to Sountoulidis et al (2023)

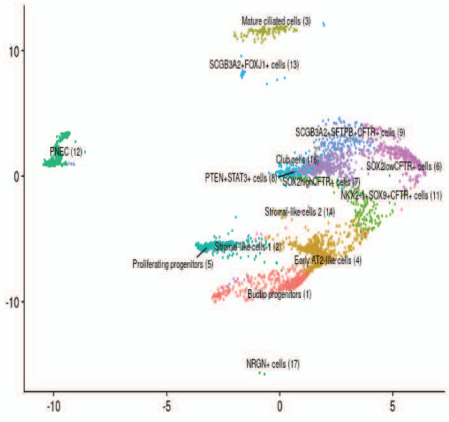

Common cell subtype	Freq
Budtip progenitors (1)	437
Club cells (16)	2
Early AT2-like cells (4)	575
Mature ciliated cells (3)	116
NKX2-1+SOX9+CFTR+ cells (11)	181
NRGN+ cells (17)	2
PNEC (12)	481
Proliferating progenitors (5)	608
PTEN+STAT3+ cells (8)	163
SCGB3A2+FOXJ1+ cells (13)	20
SCGB3A2+SFTPB+CFTR+ cells (9)	171
SOX2highCFTR+ cells (7)	493
SOX2lowCFTR+ cells (6)	341
Stromal-like cells 1 (2)	4
Stromal-like cells 2 (14)	2
Cell not found in Sountoulidis et al dataset	
Ciliated precursor cell	
SMG basal cells	
SMG secretory cells	
Basal cells	

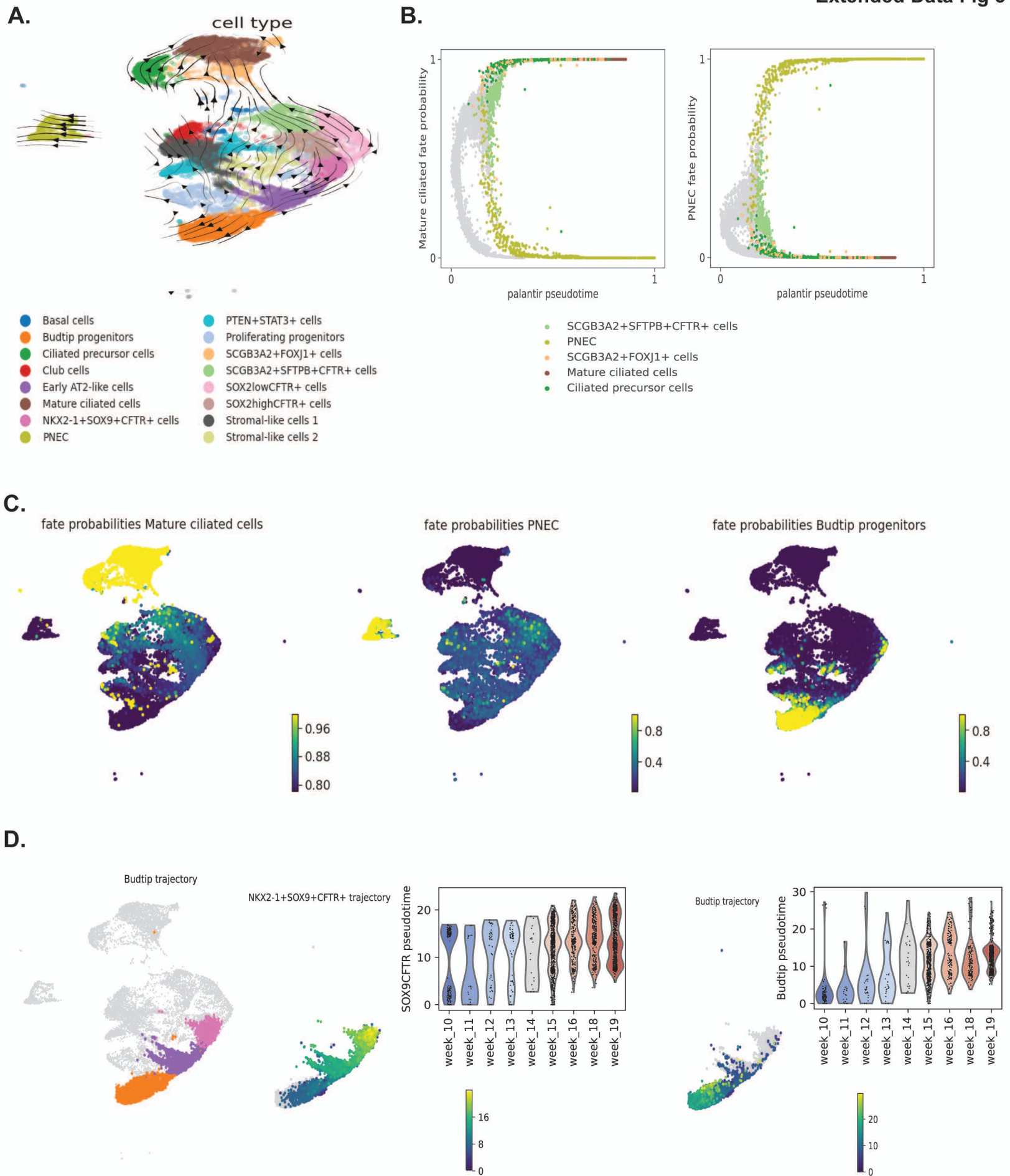
A.
cell type
Basal cells
Budtip progenitors
Ciliated precursor cells
Club cells
Early AT2-like cells
Mature ciliated cells
NKX2-1+SOX9+CFTR+ cells
PNEC
PTEN+STAT3+ cells
Proliferating progenitors
SCGB3A2+FOXJ1+ cells
SCGB3A2+SFTPB+CFTR+ cells
SOX2lowCFTR+ cells
SOX2highCFTR+ cells
Stromal-like cells 1
Stromal-like cells 2
B.
Mature ciliated fate probability
palantir pseudotime
PNEC fate probability
palantir pseudotime
SCGB3A2+SFTPB+CFTR+ cells
PNEC
SCGB3A2+FOXJ1+ cells
Mature ciliated cells
Ciliated precursor cells
C.
fate probabilities Mature ciliated cells
fate probabilities PNEC
fate probabilities Budtip progenitors
D.
Budtip trajectory
NKX2-1+SOX9+CFTR+ trajectory
SOX9CFTR pseudotime
week_10
week_11
week_12
week_13
week_14
week_15
week_16
week_18
week_19
Budtip trajectory
Budtip pseudotime

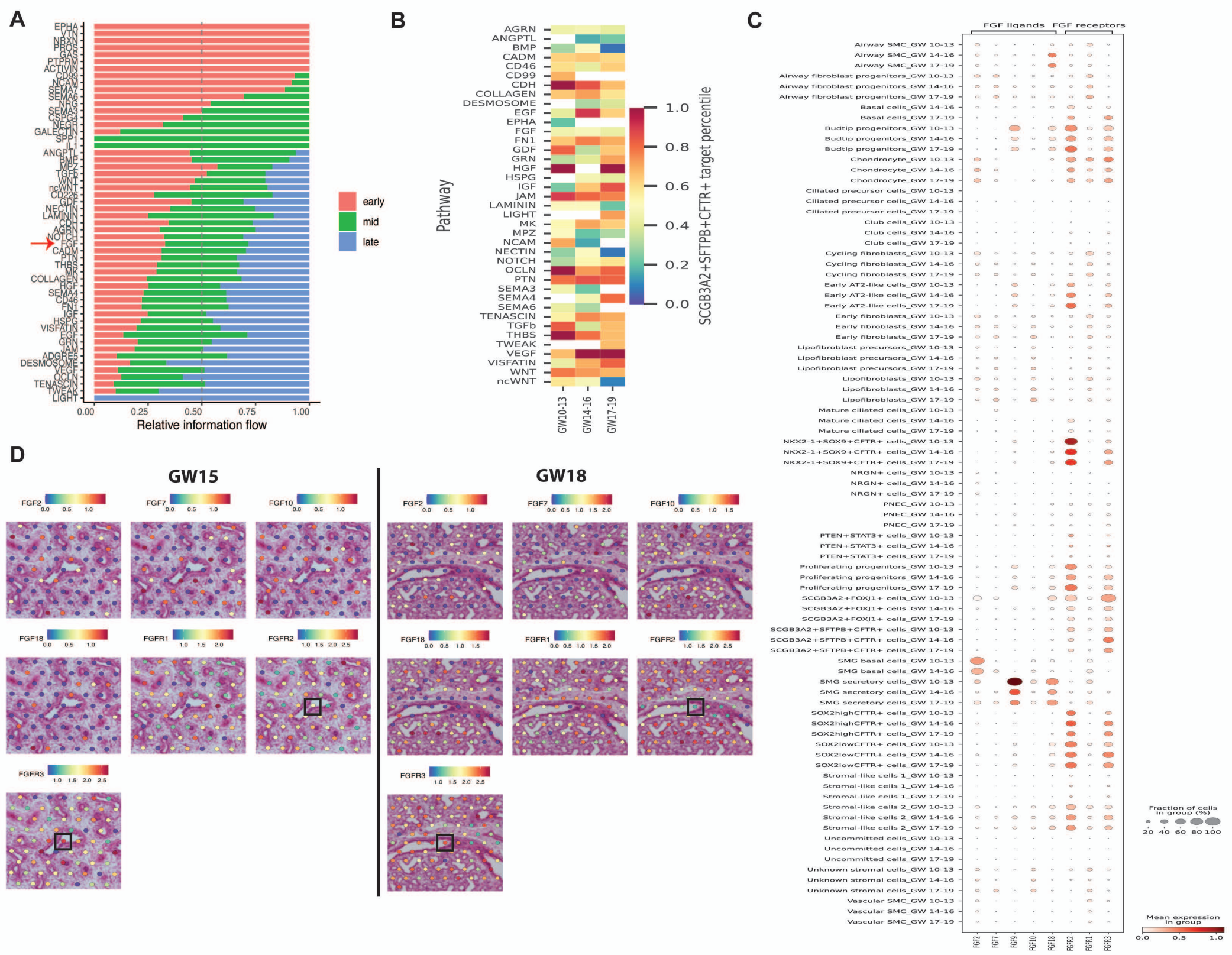
A
EPHA
PTN
NRXN
PROS
GAS
PTPRM
ACTIVIN
CD99
NCAM
SEMA7
SEMA6
NRG
SEMA3
CSPG4
NEGR
GALECTIN
SPP1
IL1
ANGPTL
BMP
MPZ
TGFb
WNT
ncWNT
CD226
GDF
NECTIN
LAMININ
CDH
AGRN
NOTCH
FGF
CADM
PTN
THBS
MK
COLLAGEN
HGF
SEMA4
CD46
FN1
IGF
HSPG
VISFATIN
EGF
GRN
JAM
ADGRE2
DESMOSOME
VEGF
OCLN
TENASCIN
TWEAK
LIGHT
0.00
0.25
0.50
0.75
1.00
Relative information flow
early
mid
late
B
Pathway
AGRN
ANGPTL
BMP
CADM
CD46
CD99
CDH
COLLAGEN
DESMOSOME
EGF
EPHA
FGF
FN1
GDF
GRN
HGF
HSPG
IGF
JAM
LAMININ
LIGHT
MK
MPZ
NCAM
NECTIN
NOTCH
OCLN
PTN
SEMA3
SEMA4
SEMA6
TENASCIN
TGFb
THBS
TWEAK
VEGF
VISFATIN
WNT
ncWNT
GW10-13
GW14-16
GW17-19
1.0
0.8
0.6
0.4
0.2
0.0
SCGB3A2+SFTPB+CFTR+ target percentile
C
FGF ligands
FGF receptors
Airway SMC_GW 10-13
Airway SMC_GW 14-16
Airway SMC_GW 17-19
Airway fibroblast progenitors_GW 10-13
Airway fibroblast progenitors_GW 14-16
Airway fibroblast progenitors_GW 17-19
Basal cells_GW 14-16
Basal cells_GW 17-19
Budtip progenitors_GW 10-13
Budtip progenitors_GW 14-16
Budtip progenitors_GW 17-19
Chondrocyte_GW 10-13
Chondrocyte_GW 14-16
Chondrocyte_GW 17-19
Ciliated precursor cells_GW 10-13
Ciliated precursor cells_GW 14-16
Ciliated precursor cells_GW 17-19
Club cells_GW 10-13
Club cells_GW 14-16
Club cells_GW 17-19
Cycling fibroblasts_GW 10-13
Cycling fibroblasts_GW 14-16
Cycling fibroblasts_GW 17-19
Early AT2-like cells_GW 10-13
Early AT2-like cells_GW 14-16
Early AT2-like cells_GW 17-19
Early fibroblasts_GW 10-13
Early fibroblasts_GW 14-16
Early fibroblasts_GW 17-19
Lipofibroblast precursors_GW 10-13
Lipofibroblast precursors_GW 14-16
Lipofibroblast precursors_GW 17-19
Lipofibroblasts_GW 10-13
Lipofibroblasts_GW 14-16
Lipofibroblasts_GW 17-19
Mature ciliated cells_GW 10-13
Mature ciliated cells_GW 14-16
Mature ciliated cells_GW 17-19
NKX2-1+SOX9+CFTR+ cells_GW 10-13
NKX2-1+SOX9+CFTR+ cells_GW 14-16
NKX2-1+SOX9+CFTR+ cells_GW 17-19
NRGN+ cells_GW 10-13
NRGN+ cells_GW 14-16
NRGN+ cells_GW 17-19
PNEC_GW 10-13
PNEC_GW 14-16
PNEC_GW 17-19
PTEN+STAT3+ cells_GW 10-13
PTEN+STAT3+ cells_GW 14-16
PTEN+STAT3+ cells_GW 17-19
Proliferating progenitors_GW 10-13
Proliferating progenitors_GW 14-16
Proliferating progenitors_GW 17-19
SCGB3A2+FOXJ1+ cells_GW 10-13
SCGB3A2+FOXJ1+ cells_GW 14-16
SCGB3A2+FOXJ1+ cells_GW 17-19
SCGB3A2+SFTPB+CFTR+ cells_GW 10-13
SCGB3A2+SFTPB+CFTR+ cells_GW 14-16
SCGB3A2+SFTPB+CFTR+ cells_GW 17-19
SMG basal cells_GW 10-13
SMG basal cells_GW 14-16
SMG secretory cells_GW 10-13
SMG secretory cells_GW 14-16
SMG secretory cells_GW 17-19
SOX2highCFTR+ cells_GW 10-13
SOX2highCFTR+ cells_GW 14-16
SOX2highCFTR+ cells_GW 17-19
SOX2lowCFTR+ cells_GW 10-13
SOX2lowCFTR+ cells_GW 14-16
SOX2lowCFTR+ cells_GW 17-19
Stromal-like cells 1_GW 10-13
Stromal-like cells 1_GW 14-16
Stromal-like cells 1_GW 17-19
Stromal-like cells 2_GW 10-13
Stromal-like cells 2_GW 14-16
Stromal-like cells 2_GW 17-19
Uncommitted cells_GW 10-13
Uncommitted cells_GW 14-16
Uncommitted cells_GW 17-19
Unknown stromal cells_GW 10-13
Unknown stromal cells_GW 14-16
Unknown stromal cells_GW 17-19
Vascular SMC_GW 10-13
Vascular SMC_GW 14-16
Vascular SMC_GW 17-19
FGF2
FGF7
FGF9
FGF10
FGF18
FGFR2
FGFR1
FGFR3
Fraction of cells in group (%)
20 40 60 80 100
Mean expression in group
0.0 0.5 1.0
D
GW15
GW18
FGF2
FGF7
FGF10
FGF18
FGFR1
FGFR2
FGFR3

Extended Data Fig 7

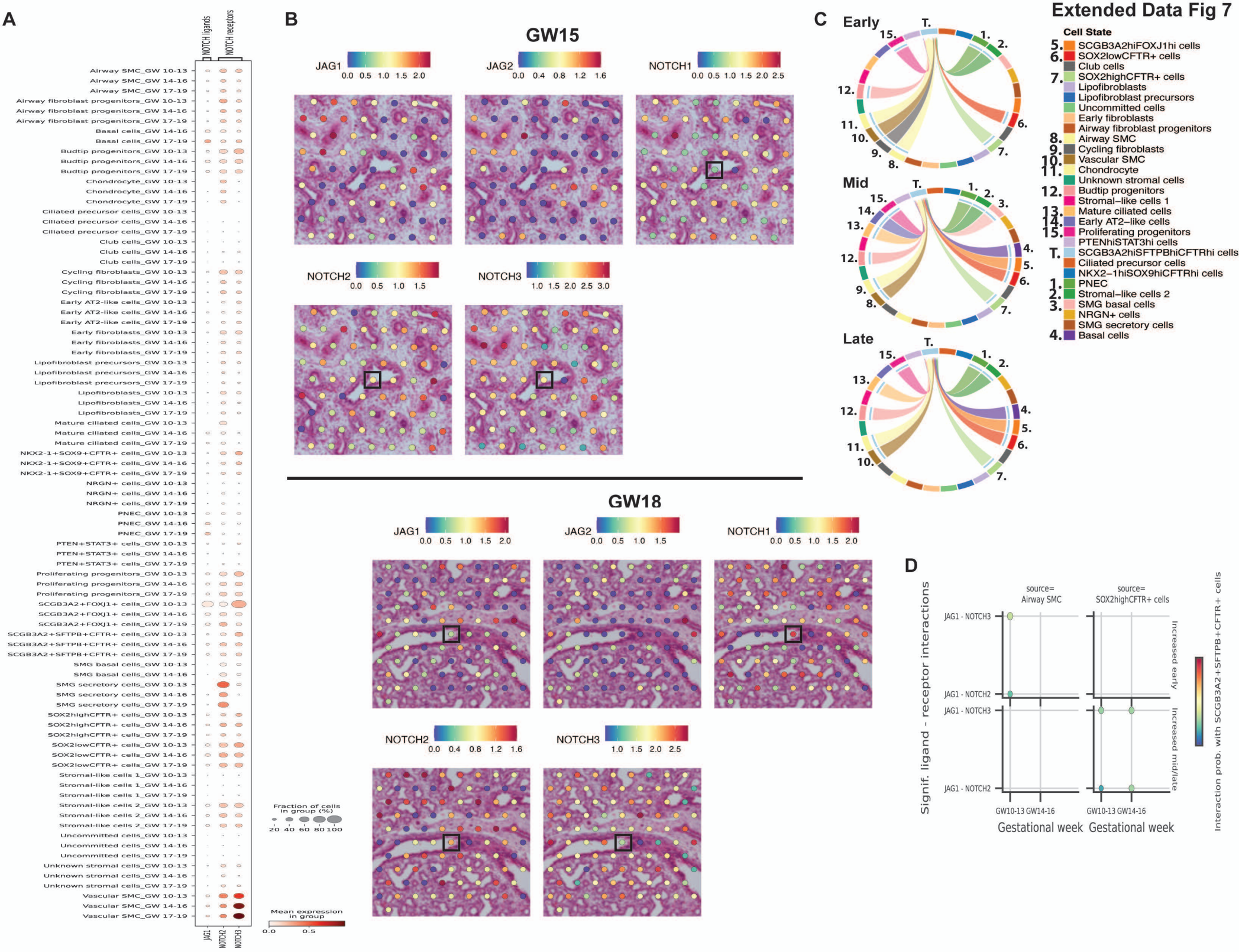
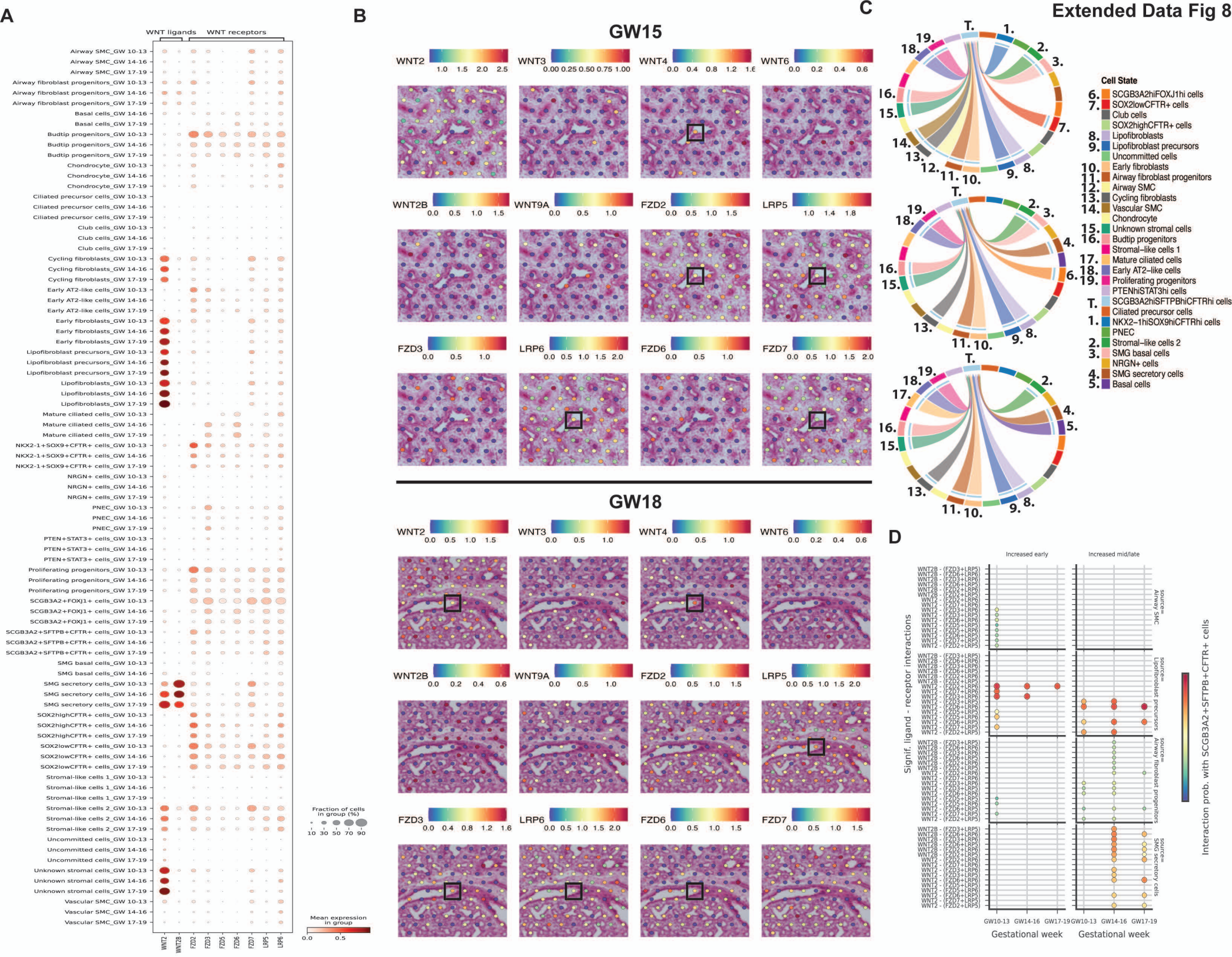
Extended Data Fig 8